

THE FLORIDA STATE UNIVERSITY
COLLEGE OF ARTS AND SCIENCES

EVALUATING OPERATIONAL AND NEWLY DEVELOPED
MESOCYCLONE AND TORNADO DETECTION ALGORITHMS
FOR QUASI-LINEAR CONVECTIVE SYSTEMS

By

THOMAS JAMES TURNAGE

A thesis submitted to the
Department of Meteorology
in partial fulfillment of the
requirements for the degree of
Master of Science

Degree Awarded:
Summer Semester, 2007

The members of the Committee approve the thesis of Thomas J. Turnage defended on April 5th, 2007.

Henry E. Fuelberg
Professor Directing Thesis

Jon E. Ahlquist
Committee Member

Paul H. Ruscher
Committee Member

Andrew I. Watson
Committee Member

The Office of Graduate Studies has verified and approved the above named committee members.

ACKNOWLEDGEMENTS

I first want to thank the Lord. Without His blessings, none of this would have been possible. Next, I want to express my deepest gratitude and appreciation to my major professor Dr. Henry Fuelberg for working with me to complete this thesis in spite of rotating shift work at the National Weather Service (NWS) in Tallahassee and a subsequent move to Michigan. His high standards of integrity and academic excellence have been an inspiration to me. I also wish to thank the members of my thesis committee, Mr. Irv Watson of the NWS in Tallahassee, and Drs. Jon Ahlquist and Paul Ruscher for their advice and support. I am especially grateful to my colleague Irv, who always was very supportive of my research efforts.

Thank you to the entire NWS staff at Tallahassee, who covered for me on many occasions so I could pursue this goal. My former supervisor, Paul Duval, was especially supportive, for which I am very grateful. Both past and present members of the Fuelberg lab have helped me tremendously with various aspects of my research. Thanks especially to Phil Shafer for his advice with statistics and instruction with the S-PLUS software package. I am also very grateful to Valliappa Lakshmanan at the National Severe Storms Laboratory for helping me to acquire and utilize the WDSSII software for my research.

I would like to thank my parents for their love and support, and for giving me a love of learning and academics. Finally, I am deeply grateful to my wife Sarah for her unconditional love, support, and selflessness that made it possible for me to complete this endeavor.

TABLE OF CONTENTS

List of Tables	v
List of Figures	vii
Abbreviations and Acronyms	x
Abstract	xi
1. INTRODUCTION	1
2. DATA AND METHODOLOGY	6
2.1 Definitions	6
2.2 Methodology	6
2.3 Cases	11
3. RESULTS	14
3.1 Severe Storms Analysis Package (SSAP) data	14
3.2 Regression Tree Models	21
3.3 Additional parameters	29
3.3.1 Spectrum Width	31
3.3.2 Azimuthal Shear	41
3.3.3 Reflectivity Variance	49
4. SUMMARY AND CONCLUSIONS	60
REFERENCES	64
BIOGRAPHICAL SKETCH	67

LIST OF TABLES

Table 1. Native and operational resolution of WSR-88D products. Native resolutions are generated by the radar software. Operational resolutions are available to forecasters in a real-time environment. For all products, the beam width is 1 degree. Maximum resolvable radial lengths are given in km.....	3
Table 2. Tornado episodes and events.....	11
Table 3. TVS and mesocyclone detections.....	12
Table 4. Tornadic and pre-tornadic detections before and during tornado occurrences. Numbers in the top row denote the number of scans prior to the tornado, following the convention in Fig. 3 and Fig. 4. Tornado occurrence is denoted by zero.	13
Table 5. Distribution of confidence levels assigned to all mesocyclone or TVS detections associated with an occurring or imminent tornado. Numbers in the top row range from 1 (low confidence) to 3 (high confidence).	13
Table 6. Initial SSAP Predictors used for QLCS tornadoes.	15
Table 7. Correlation coefficients for the M0 matrix in Fig. 10.....	19
Table 8. As in Table 7, except for the MPRE matrix in Fig. 11.	20
Table 9. Correlation coefficients for the MDA SSAP parameters listed in Table 6. Coefficients above the gray diagonal are for the non-tornadic mesocyclone detection (NTM) versus tornadic mesocyclone detection (M0) datasets. Coefficients below the diagonal are for the NTM versus pre-tornadic mesocyclone detection (MPRE) datasets.	22
Table 10. As in Table 9, except for the TDA SSAP parameters. The comparison above the gray diagonal is for non-tornadic TVS detections (NTT) versus tornadic TVS detections (T0) and below the diagonal is NTT versus pre-tornadic TVS detections (TPRE).	22
Table 11. Modified list of SSAP diagnostics. Yes or No indicates whether the diagnostic was used for regression trees. NA means the diagnostic is not available.	23
Table 12. Additional non-SSAP parameters.....	31
Table 13. KS values (top rows) and p-values of confidence (bottom rows) from two-sample Kolmogorov-Smirnov goodness of fit tests for different array sizes of SW. The compared samples are listed in the left column.	32
Table 14. Correlation coefficients the different arrays of MALL SW.	38
Table 15. As in Table 14, except for NTM detections.	38
Table 16. As in Table 14, except for MPRE detections.....	39
Table 17. As in Table 14, except for M0 detections	39
Table 18. Regression tree inclusion matrix for SW arrays. Arrays appearing in regression trees are denoted with a “Yes”. The numbers below each Yes designation indicate the split in which the SW array appeared. The following number indicates the threshold at which the split occurred in $m s^{-1}$	39
Table 19. As in Table 13, except for different array sizes of Azimuthal Shear (AZ).	46

Table 20. As in Table 18, except for AZ in units of ($10^{-4} \times \text{s}^{-1}$)..... 46

Table 21. Correlation coefficients for the REV arrays. Coefficients above the gray diagonal are for the tornadic and pre-tornadic mesocyclone detection (MALL) datasets. Coefficients below the diagonal are for the NTM datasets. 55

Table 22. Correlation coefficients for the REV arrays. Coefficients above the gray diagonal are for the MPRE datasets. Coefficients below the diagonal are for the M0 datasets..... 55

Table 23. As in Table 13, except for REnV arrays. 56

Table 24. As in Table 18, except for REnV arrays. 57

Table 25. Results for regression trees including SWn and REnV arrays. The first line indicates whether REV or SW appears in the regression tree. The second line indicates at which split the parameter occurs. The third line indicates the threshold of the split..... 58

LIST OF FIGURES

Fig 1. Schematic showing how a mesocyclone or TVS consists of multiple 2-dimensional segments in different radar elevation slices. Figure taken from Mitchell et al. (1988).....	2
Fig. 2. Plan views of Reflectivity (top left), Storm Relative Motion (top right), Spectrum Width (bottom left), and Azimuthal Shear (bottom right) at the 0.5 degree elevation slice for approximately the same time. The radar location is depicted by the black disk near the upper center of each image. Confirmed tornado locations are indicated by the time labels, which depict the corrected start time in UTC. A tornado is about to develop just northwest of the radar near the 1128 UTC time label.....	5
Fig. 3. Time correction of tornado starting and ending locations. The shaded ovals represent the 0.5 degree elevation SRM inbound /outbound couplet for a sequence of volume scans. The first number below each couplet is the scan number relative to the tornado start or end time (0 is during the tornado). Below the scan is the time the velocity data were recorded by the radar.....	8
Fig. 4. Time correction for a case when the couplet strengthens significantly, shown schematically by the larger couplet, and then weakens again in the following scan. The Storm Data start and end locations are nearly identical, with the strengthening occurring immediately downstream. In this case, the tornado start and ending times are assumed to be nearly identical and associated with the scan containing the strongest couplet.....	9
Fig. 5. Tornado event start locations and WSR-88Ds used in the dataset.....	12
Fig. 6. LLDV quartile box plots. MALL is all mesocyclones during and up to 4 volume scans prior to the QLCS tornadoes. M0 is all mesocyclones during the tornado. M1 through M4 are mesocyclones occurring during volume scans 1 through 4 prior to the tornado. MPRE is the collection of pre-tornado mesocyclones for scans 1 through 4. Non-tornadic mesocyclones comprising the null set are denoted by NTM. TPRE, T0, TALL, and NTT are similarly denoted, except for TVS detections.....	16
Fig. 7. As in Fig. 6, except for Strength Index. Units are dimensionless.....	17
Fig. 8. As in Fig. 6, except for LLROTV. Note the smaller velocity scale. Since TDA LLROTV diagnostics do not exist, they could not be included.....	17
Fig. 9. As in Fig. 6, except for LLCONV.....	18
Fig. 10. Scatter plot matrix for Mesocyclone LLDV, MXDV, LLROTV, and MXROTV during tornado occurrence (M0). All units in $m s^{-1}$	19
Fig. 11. As in Fig. 10, except prior to tornado occurrence (MPRE).....	20
Fig. 12. Deviance measured from a 10-fold cross validation of the NTM versus M0 regression tree.....	24
Fig. 13. As in Fig. 12, except for the NTT versus T0 regression tree.....	24
Fig. 14. Regression tree for Non-Tornadic Mesocyclone (NTM) versus Mesocyclone detections during tornado occurrence (M0). In this case, Vertically Integrated Rotational Velocity (VIROTV) is the parameter best able to discriminate between the NTM and M0 datasets. If $VIROTV < 11.0 m s^{-1}$, there is a 0.9% percent chance of the detection being an M0 detection. If $VIROTV \geq 11.0 m s^{-1}$, then Low-Level Delta Velocity (LLDV) is the next most effective parameter to discriminate between the datasets. The number at the end of each branch	

denotes the ratio of M0 detections for the set of conditions leading to the branch.....	25
Fig. 15. Regression tree with 4 terminal nodes for NTM versus MPRE detections.	25
Fig. 16. Regression tree for NTM versus MALL detections.	26
Fig. 17. Regression tree for NTT versus T0 detections.....	27
Fig. 18. Regression tree for NTT versus TPRE detections.	28
Fig. 19. Schematic of a data array. The dark box marked by an "X" corresponds to the range gate and azimuth associated with the centroid of the detection. The centroid plus the lighter shaded boxes represent the area over which means and variances are calculated for the centroid location. This particular example represents a 5 X 5 array, i.e., an array size of 5.	30
Fig. 20. Probability distribution histograms for the different SW array sizes from the NTM dataset. Units on the abscissa are in $m s^{-1}$	32
Fig. 21. As in Fig. 20, except from the MALL dataset.	33
Fig. 22. As in Fig. 20, except from the NTT dataset.....	33
Fig. 23. As in Fig. 20, except from the TALL dataset.	34
Fig. 24. As in Fig. 6, except for SW.	35
Fig. 25. As in Fig. 6, except for SW5.....	36
Fig. 26. Scatter plot correlation matrix for all arrays of MALL SW.	38
Fig. 27. Regression tree for NTT versus T0 detections using the TVS parameters in Table 6 with SW9.....	40
Fig. 28. As in Fig. 20 and Fig. 21, except for Azimuthal Shear with Non-Tornadic Mesocyclones (NTM) and all Tornadic/Pre-tornadic Mesocyclones (MALL).	42
Fig. 29. As in Fig. 22 and Fig. 23, except for Azimuthal Shear with Non-Tornadic TVS detections (NTT; top) and all Tornadic/pre-tornadic TVS detections (TALL; bottom). Array sizes from left to right are 1,5, and 7.	43
Fig. 30. As in Fig. 20, except for AZ arrays with M0 and T0 datasets.....	44
Fig. 31. As in Fig. 6, except for AZ.	44
Fig. 32. As in Fig. 31, except for AZ5.....	45
Fig. 33. As in Fig. 31, except for AZ7.	45
Fig. 34. As in Fig. 14, except including AZ5 in units of $10^{-4} s^{-1}$	47
Fig. 35. NTT versus TALL comparison with TDA parameters (Table 11) and including AZ5 in of units of $10^{-4} s^{-1}$	48
Fig. 36. Schematic of two 5 X 5 arrays of Reflectivity. Darker blocks represent radar bins with relatively large values of Reflectivity. Both arrays have equal variances, but unequal gradients of Reflectivity.	49
Fig. 37. As in Fig. 20, except for REV. The arrays are labeled RE#V, where # is the array size	

(see Fig. 36 for an illustration of array sizes). The top row is non-tornadic mesocyclones (NTM), the bottom row is tornadic/pre-tornadic mesocyclones (MPRE), and array sizes from left to right are 5,7,9, and 11. 50

Fig. 38. As in Fig. 37, except for NTT (top) and TALL (bottom). 51

Fig. 39. As in Fig. 37, except for M0 (top) and T0 (bottom). 52

Fig. 40. As in Fig. 6, except for RE5V. 53

Fig. 41. As in Fig. 6, except for RE7V. 53

Fig. 42. As in Fig. 6, except for RE9V. 54

Fig. 43. As in Fig. 6, except for RE11V. 55

Fig. 44. NTT versus TALL regression tree using SSAP TVS parameters from Table 6 with RE11V. 57

Fig. 45. NTT versus T0 regression tree using SSAP TVS parameters from Table 6 with SW9 and RE9V. 59

ABBREVIATIONS AND ACRONYMS

API	Application Programming Interface
ARL	Above Radar Level
AZ	Azimuthal Shear
HMXDV	Height of Maximum Delta-V (km)
LLCONV	Low-Level Convergence
LLDV	Low-Level Delta Velocity
LLROTV	Low-Level Rotational Velocity
LLSD	Linear Least Squares Derivative
M0	Mesocyclone detection during tornado [scan(s) 0]
M1,M2,...M4	Mesocyclone detection at scans 1-4 prior to tornado scan time(s)
M03	Manross et al. 2003
MALL	all tornadic and pre-tornadic Mesocyclone detections (scans 0-4)
MPRE	all pre-tornadic Mesocyclone detections (scans 1-4)
MDA	Mesocyclone Detection Algorithm
MSI	Mesocyclone Strength Index
MXROTV	Maximum Rotational Velocity
MXDV	Maximum Delta-V
NCDC	National Climate Data Center
NSSL	National Severe Storms Laboratory
NSE	Near-Storm Environment
NTM	Non-Tornadic (and non-pretornadic) mesocyclone
NTT	Non-Tornadic (and non-pretornadic) TVS
NWS	National Weather Service
QLCS	Quasi-Linear Convective System
RAN	Range in kilometers from the radar
RDA	Radar Data Acquisition
RE	Reflectivity
REV	Reflectivity Variance
ROTV	Rotational Velocity
SI	Strength Index
SRM	Storm Relative Motion
SW	Spectrum Width
SSAP	Severe Storms Analysis Package
T0	TVS detection during tornado [scan(s) 0]
T1,T2...T4	TVS detection at scans 1-4 prior to tornado scan time(s)
TALL	all tornadic and pre-tornadic TVS detections (scans 0-4)
TPRE	all pre-tornadic TVS detections (scans 1-4)
TDA	Tornado Detection Algorithm
TSI	Tornado Strength Index
TVS	Tornado Vortex Signature
VCP	Volume Coverage Pattern
VIDV	Vertically Integrated Delta Velocity
VIROTV	Vertically Integrated Rotational Velocity
VISHR	Vertically Integrated Shear
WDSSII	Warning Decision Support System – Integrated Information
WSR-88D	Weather Surveillance Radar – 1988 Doppler

ABSTRACT

Tornadoes in the southeastern United States frequently occur with quasi-linear convective systems (QLCSs, also referred to as squall lines). Studies have shown that the non-descending mode of tornadogenesis (i.e., when strong rotation with a tornado builds upward through the storm) is especially common with the QLCS. Due to the frequent non-descending mode of tornadogenesis associated with QLCS tornadoes (hereafter referred to as tornadoes), it is difficult to issue timely tornado warnings for them.

86 tornadoes associated with QLCS systems that occurred during 22 separate severe weather episodes were studied using archived Warning Surveillance Radar – 1988 Doppler (WSR-88D) data to recreate mesocyclones and Tornado Vortex Signatures (TVSs) identified by the WSR-88D operational algorithms. Storm Data reports were used to create separate datasets of tornadic, pre-tornadic, and non-tornadic (null) mesocyclone and TVS detections.

Selected diagnostics from the Mesocyclone and TVS Detection Algorithms (MDA and TDA, respectively) were compared between the tornadic and non-tornadic datasets. Low Level Delta Velocity (LLDV), Low-Level Rotational Velocity (LLROTV), and Strength Index (SI) showed some skill at discriminating between the tornadic and non-tornadic mesocyclones; however, the remainder of the selected mesocyclone parameters showed no significant skill, and none of the TVS parameters showed significant skill at discriminating between the tornadic, non-tornadic, or pre-tornadic cases. For mesocyclones, a correlation coefficient of 0.803 between LLDV and Maximum Delta Velocity for the pre-tornadic detections suggested that most of the tornadoes followed the non-descending tornadogenesis paradigm.

Selected MDA and TDA diagnostics were combined using regression trees to determine whether these combinations would improve the skill at discriminating between tornadic and non-tornadic mesocyclones and TVSs. Ten-fold cross validation tests were performed on the selected diagnostics to ensure that the regression trees would generalize to independent data. Vertically Integrated Rotational Velocity and LLDV most often were selected for the regression trees. Some combinations of predictors produced detection success rates exceeding 30%, thereby exceeding the success rates when single MDA or TDA parameters were used.

Various sized arrays of Spectrum Width (SW), Azimuthal Shear (AZ), and Reflectivity (RE) were combined with the MDA and TDA diagnostics to determine if these predictors contributed additional skill at discriminating tornadic mesocyclones and TVSs from the non-tornadic variety. These parameters had not been considered in previous studies.

Qualitative analysis showed that the largest values of SW occurred with the non-tornadic dataset, but the differences between this dataset and the tornadic datasets were too small to be useful in an operational setting. Two sample Kolmogorov-Smirnov goodness-of-fit tests revealed that, in general, statistically significant differences did not exist among tornadic, pre-tornadic, and non-tornadic datasets for the different array sizes. Generally, qualitative differences were smallest with the largest arrays.

SW arrays were included in the list of selected MDA and TDA diagnostics to create regression trees that would determine whether these combinations would yield predictive skill comparable to the best performing MDA and TDA diagnostics. For the mesocyclone detections, the same predictors (VIROTV and LLDV) dominated every SW array size. For the TVS comparisons, only the larger SW arrays appeared in some trees. This suggests that the larger SW arrays had predictive ability that was comparable to the four TDA predictors used in the regression trees

Azimuthal Shear (AZ) frequently was found to exhibit negative values, even at the times of tornado occurrence. This result was unexpected since mesocyclones and TVSS are almost always associated with positive shear. Different array sizes of AZ showed strong correlations with each other, which was expected since the linear least squares derivative that is applied to the Velocity data has an *a priori* smoothing effect. Two-sample Kolmogorov-Smirnov goodness-of-fit tests showed that the most statistically significant differences in AZ occurred between the non-tornadic mesocyclones (NTM) and both the tornadic mesocyclones (M0) and the tornadic/pre-tornadic mesocyclones (MALL). Results indicated that AZ exhibited less ability than SW as a sole predictor at discriminating between tornadic and non-tornadic mesocyclones. However, when used in regression trees together with MDA and TDA parameters, AZ exhibited utility comparable to SW for TVS detections and was superior to SW for mesocyclone detections. When both SW and AZ arrays were used to create regression trees, SW always emerged as the dominant predictor. A surprising finding was the preponderance of negative AZ values in the tornadic TVS detections.

Increasing array sizes of Reflectivity Variance (REV) appeared to have an upper limit of utility. Contrary to what was hypothesized, pre-tornadic mesocyclone and TVS detections exhibited larger variances than tornadic detections. Based on two-sample Kolmogorov-Smirnov goodness-of-fit tests, only the non-tornadic mesocyclone (NTM) versus pre-tornadic mesocyclone (MPRE) datasets exhibited statistically significant differences. None of the other comparisons was statistically significant. REV did not exhibit skill comparable to the best Severe Storms Analysis Package (SSAP) diagnostics for the mesocyclone detections in the regression trees that were constructed. However, for TVS detections, the larger REV arrays appeared in regression trees for the NTT versus TALL comparisons, and smaller arrays appeared in regression trees for

the NTT versus TPRES comparisons. Regression trees combining REV arrays with the best-performing MDA and TDA predictors showed that REV exhibited better predictive ability for the TVS datasets compared to SW and AZ.

These results suggest that SW, AZ, and REV all show utility as predictors when used in combination with some of the already existing MDA and TDA diagnostic parameters. Incorporating these additional data sources into the algorithms therefore could improve their performance.

CHAPTER ONE

Introduction

The tornado is a relatively rare atmospheric phenomenon that is capable of producing significant destruction and casualties. The tornado's relatively small spatial scale usually makes it impossible to resolve explicitly with weather surveillance radar. Fortunately, tornadoes often are preceded by a larger storm-scale circulation, called the mesocyclone. With the advent of the Weather Surveillance Radar – 1988 Doppler (WSR-88D) in the National Weather Service (NWS), it has become possible to detect potentially pre-tornadic circulations using both the Mesocyclone Detection Algorithm (MDA; Stumpf et al. 1998) and the Tornado Detection Algorithm (TDA; Mitchell et al. 1998). The MDA and TDA are components of the Severe Storm Analysis Package (SSAP) developed by the National Severe Storms Laboratory (NSSL) in Norman, Oklahoma. The TDA infers the existence of a tornado based on a Tornado Vortex Signature (TVS) which denotes sufficient rotation at the smallest resolvable scale of the radar. The MDA has shown excellent skill at detecting mesocyclones; however, observations indicate that relatively few mesocyclones are associated with tornadoes (Stumpf et al. 1998; Jones et al. 2004; Trapp et al. 2005). The mesocyclones and TVVs that are detected are 3-dimensional features that consist of a series of stacked 2-dimensional segments, with each 2-dimensional segment consisting of an area on a radar elevation slice where sufficient cyclonic shear is detected (Fig. 1).

Several recent studies (e.g., Trapp et al. 1999; Funk et al. 1999) have shown that many radar-observed tornadic circulations originate in the lowest levels of thunderstorms. These circulations then rapidly strengthen and stretch upward with the onset of the tornado. This is a very different scenario from the classical radar-observed tornadogenesis paradigm introduced by Brown et al. (1978) in which the strongest circulations originate in the middle levels of the storm as a mesocyclone, which then stretch and intensify toward the surface as a tornado via the dynamic pipe effect described by Leslie (1971). Conversely, numerical simulations by Trapp and Davies-Jones (1997) strongly suggest that the strongest rotation with the non-descending mode of tornadogenesis begins and remains in the lowest levels of the storm.

The non-descending mode of tornadogenesis is especially common within quasi-linear convective systems (QLCSs; Tessendorf and Trapp 2000), even during strongly forced events (e.g., Turnage et al. 2000). Using the definition of Tessendorf and Trapp, a QLCS is “a quasi-linear region of radar reflectivity greater than or equal to 40 dBz, continuously distributed over a horizontal distance greater than 100 km.” This definition excludes cases characterized by a row of closely spaced discrete cells. Due to the frequent low-level origin and rapid onset of QLCS

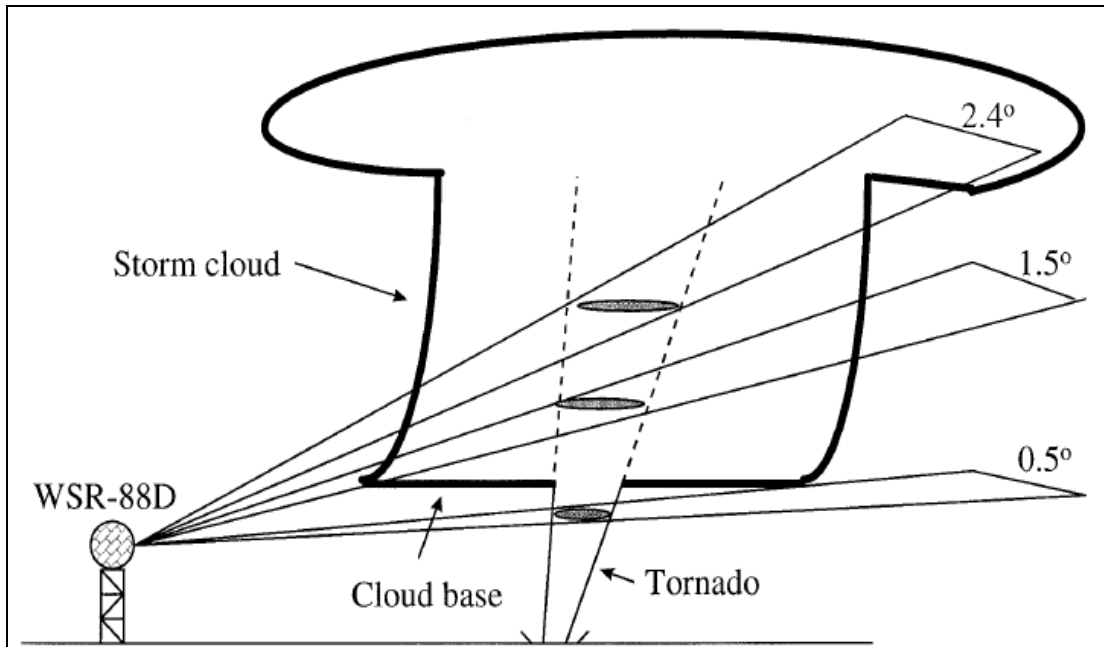


Fig 1. Schematic showing how a mesocyclone or TVS consists of multiple 2-dimensional segments in different radar elevation slices. Figure taken from Mitchell et al. (1988).

tornadoes, it is difficult to issue timely tornado warnings for them, even though the simulations suggest that the strength and general dimensions of the QLCS mesocyclone approximate those of the classical tornado mesocyclone (Weisman and Trapp 2003).

Although a mesocyclone identified by the MDA is in itself a poor tornado predictor, certain mesocyclone vortex diagnostic measurements associated with the MDA have shown skill at differentiating between tornadic and non-tornadic circulations. One such measurement is Rotational Velocity (ROTV), defined as the average of the magnitudes of the maximum inbound and outbound velocities of the mesocyclone circulation. Several studies (e.g., Watson et al. 2005; Marzban 2001; Turnage et al. 2000) have indicated that the tornado detection skill of ROTV is maximized around 20 m s^{-1} . Values of ROTV larger than this are associated with a greater probability of tornadoes; however, they are less likely to be observed, resulting in decreased probability of detection. The attainment of the 20 m s^{-1} threshold suggests, but does not necessarily imply, the existence of a tornado. Other diagnostic measurements such as the Mesocyclone Strength Index (MSI) and Maximum delta-Velocity (MXDV) were found by Jones et al. (2004) to have similar skill in differentiating between tornadic and non-tornadic mesocyclones.

Using MDA diagnostic measurements, Manross et al. (2003; hereafter M03) compared differences between supercell and QLCS tornadoes that occurred during 1998 and 1999. QLCS tornadic mesocyclones were found to be shallower and lower in altitude, and to have somewhat stronger Low-Level Convergence (LLCONV). They also found that rotational characteristics of

QLCS tornadic mesocyclones were similar to those of supercell tornado mesocyclones, except for the Low-Level Velocity Difference (LLDV) which showed greater values in the QLCS cases prior to the onset of the tornado.

Reflectivity (RE), Velocity (V), and Spectrum Width (SW) are the only three base products generated by the WSR-88D (Crum and Alberty 1993). Table 1 summarizes the operationally available resolutions of these products. Operational resolution is less than the native resolution for all products, and the number of data levels is compromised for SW. Velocity can be converted to Storm-Relative Motion (SRM) by estimating the motion vector of a storm and then subtracting it from V. This gives a better depiction of airflow patterns within a storm and facilitates detection of mesocyclones. The MDA and TDA only interrogate V from the three base products, with the requirement that a minimum threshold of RE is collocated with the mesocyclone or TVS.

Table 1. Native and operational resolution of WSR-88D products. Native resolutions are generated by the radar software. Operational resolutions are available to forecasters in a real-time environment. For all products, the beam width is 1 degree. Maximum resolvable radial lengths are given in km.

Base product	Native resolution	Operational resolution
Reflectivity (RE)	0.25 km 8 bit (256 data levels)	1.00 km 8 bit (256 data levels)
Velocity (V)	0.25 km out to 230 km 8 bit (256 data levels)	0.25 km out to 59.25 km range 0.50 km out to 115 km range 1.00 km out to 230 km range 8 bit (256 data levels)
Spectrum Width (SW)	0.25 km out to 230 km 8 bit (256 data levels)	0.25 km out to 59.25 km range 0.50 km out to 115 km range 1.00 km out to 230 km range 8 bit (256 data levels)

Numerous observational studies and simulations (e.g., Wakimoto et al. 1998, Lemon 1980, Weisman and Klemp 1982) have found that tornadoes typically are associated with a strong horizontal gradient of Reflectivity that is coincident with the tornadic circulation. This enhanced gradient yields a greater local variance of Reflectivity. Based on these findings, this author hypothesizes that tornadic detections will have larger local Reflectivity gradients compared to non-tornadic detections, resulting in greater local variances of Reflectivity for the tornadic detections. As an independently measured value, the variance of Reflectivity could potentially add information to the MDA or TDA and improve their ability to discriminate tornadic detections from non-tornadic detections.

Some studies (e.g., Morgan et al. 1998; Howieson et al. 1997; Welsh 1997; Herald and Drozd 2001) have shown SW to have utility in tornado detection. However, as discussed in some of these references, SW typically is a very noisy parameter (e.g., see Fig. 2), which can limit its usefulness for qualitative tornado diagnosis. Also, as noted by Zittel et al. (2001), SW values sometimes can be artificially large as a result of radar calibration errors. In such cases, SW could mislead the radar operator into overestimating a tornado threat.

With the development of the Warning Decision Support System – Integrated Information (WDSSII) software (Lakshmanan 2002), it is possible not only to test the ability of the MDA and TDA to predict tornadoes using archive-level II WSR-88D data (Crum and Burgess 1993), but also to use the WDSSII Application Programming Interface (API) to create new applications that extract data from the MDA and TDA detections and use it to interrogate the Reflectivity and SW datasets.

WDSSII also affords the opportunity to test the tornado detection skill of non-operational products derived from the base products. An example is the Azimuthal Shear (AZ) product obtained from a local Linear Least Squares Derivatives (LLSD) estimate of shear (Smith et al. 2003) due to local differences in V. Examples of Reflectivity (RE), Storm Relative Motion (SRM), Spectrum Width (SW), and Azimuthal Shear (AZ) products associated with a QLCS tornado are displayed in Fig. 2.

This study first will compare MDA/TDA diagnostics of tornadic mesocyclones/TVSs versus diagnostics from the non-tornadic variety to determine if a non-descending mode of tornadogenesis can be inferred or predicted. Next, the parameters SW, REV, and AZ will be analyzed to see if they contribute additional predictive skill to the diagnostic measurements. These additional parameters will be assessed at the lowest radar elevation slice directly below the 3-dimensional centroid of the detections. The study then will assess the usefulness of SSAP diagnostics for detecting QLCS tornadoes. Finally, I will determine whether the operationally unavailable measurements of SW, Reflectivity, and AZ improve forecast skill when used in conjunction with MDA and TDA diagnostic measurements. If these additional measures are shown to add value, the findings will support the implementation of these parameters in future mesocyclone and TVS detection algorithms.

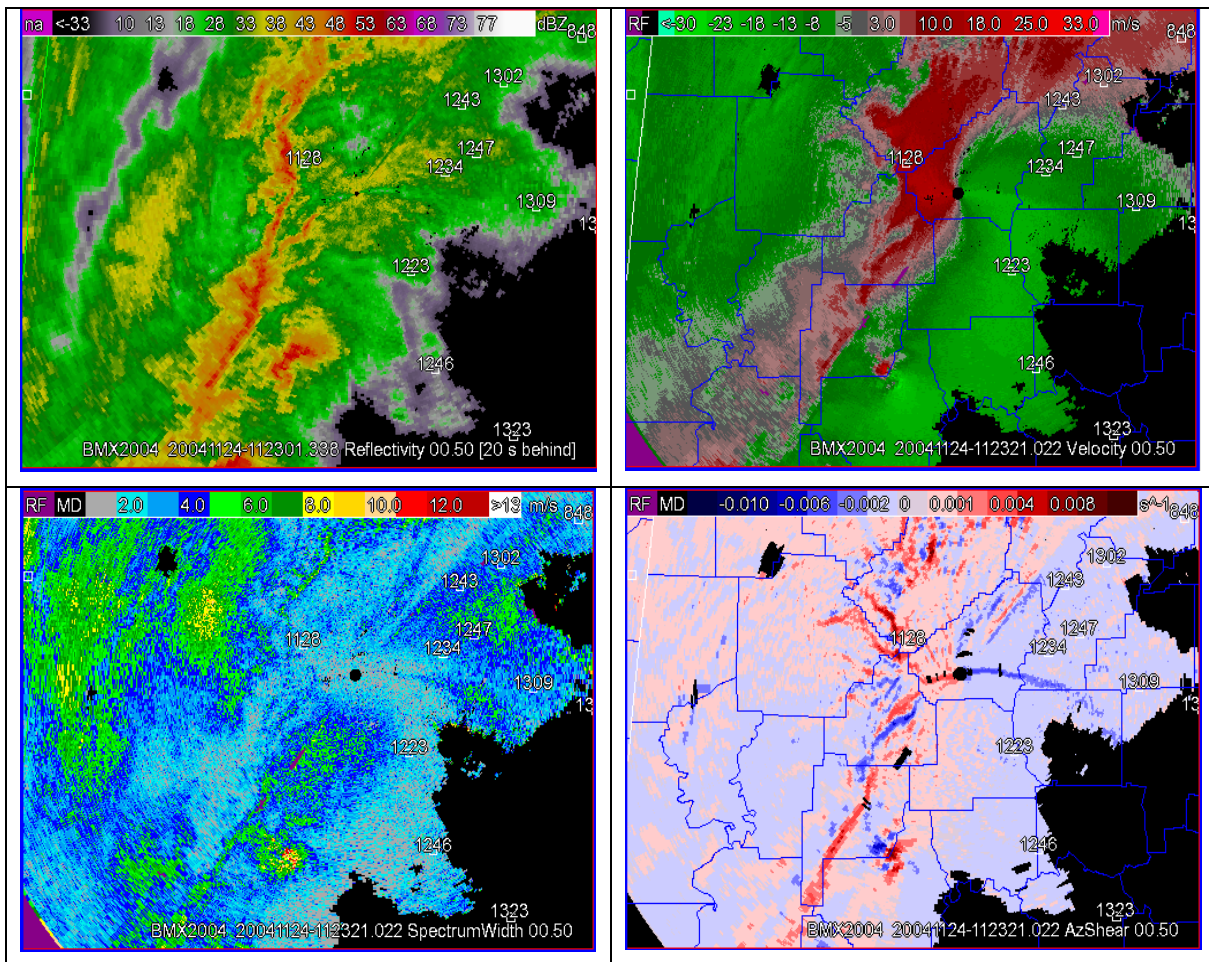


Fig. 2. Plan views of Reflectivity (top left), Storm Relative Motion (top right), Spectrum Width (bottom left), and Azimuthal Shear (bottom right) at the 0.5 degree elevation slice for approximately the same time. The radar location is depicted by the black disk near the upper center of each image. Confirmed tornado locations are indicated by the time labels, which depict the corrected start time in UTC. A tornado is about to develop just northwest of the radar near the 1128 UTC time label.

CHAPTER TWO

Data and Methodology

2.1 Definitions

Several terms must be defined for this discussion. A tornadic **detection** refers to a mesocyclone or TVS identified by the MDA or TDA which is associated with an occurring or imminent tornado. This study focuses on detections occurring during a tornado, and up to four WSR-88D volume scans prior to the tornado. A **null** detection is an identified TVS or mesocyclone not associated with an occurring or imminent tornado. A tornado **event** refers to an individual tornado occurrence that meets the requirements that follow. A tornado **episode** refers to one or more tornadoes within the observable range of a WSR-88D radar and within the time period of several hours or less. Thus, a tornado event consists of one or more detections, while an episode consists of one or more tornado events.

2.2 Methodology

The first step was to collect tornado events. Tornadic events in the southeastern and east-central United States were especially targeted because I have observed subjectively that there appears to be a relatively high frequency of QLCS tornadoes events over this region. The Tessendorf and Trapp (2000) definition of a QLCS was used, i.e., “a quasi-linear region of radar reflectivity greater than or equal to 40 dBz, continuously distributed over a horizontal distance greater than 100 km.” This definition excluded cases characterized by a line of discrete cells. Events from the M03 dataset occurring in the area of interest were used. In addition, new candidate events (i.e., events not identified in M03 but having the potential to meet the QLCS criteria) were located either by surveying web pages of NWS Warning and Forecast Offices (WFOs) in the area of interest, or by accessing Storm Data tornado reports online at the National Climatic Data Center (NCDC) website:

<http://www4.ncdc.noaa.gov/cgi-win/wwcgi.dll?wwEvent~Storms>

For each new candidate episode, the following NCDC website was used to inspect national radar reflectivity mosaic images around the hours of the tornado event:

<http://www4.ncdc.noaa.gov/cgi-win/wwcgi.dll?WWNEXRAD~Images2>

The radar imagery made it possible to determine whether each tornado event was associated with a QLCS or a discrete supercell. I assumed that the QLCS criteria already had been met for the previously-identified M03 events. However, for other episodes, all Storm Data tornado reports within a day of the episode and within ~ 150 miles of the WSR-88D locations were collected. Assuming that WSR-88D archive level II data were available for an episode, they were downloaded from NCDC to be processed in WDSSII so that base products could be displayed along with the MDA and TDA output.

There are many reasons why Storm Data reports can contain significant spatial or temporal errors (Witt et al. 1998). Therefore, it was essential to reconcile the Storm Data tornado reports with actual radar data. Each Storm Data tornado report contains the tornado's beginning and ending time, along with a location for each time in latitude and longitude. Although it is possible for a Storm Data tornado report to be erroneous with respect to both time and location, I assumed that locations likely would be more accurate because reported tornadoes often are associated with damage that frequently is surveyed.

The next step was to analyze each Storm Data tornado event to determine whether the QLCS criteria were met, and to determine whether the radar data were sufficiently complete. This step significantly reduced the number of usable QLCS tornado events from the original Storm Data reports, mainly because some tornadoes were associated with discrete cells ahead of the QLCS (e.g., as seen in Fig. 2).

Since WDSSII uses shapefiles for map backgrounds, I could use ESRI's ArcMap computer application (<http://www.esri.com>) to create background maps containing Storm Data tornado starting and ending point latitude/longitude coordinates. Using the premise that the starting and ending locations were accurate, the radar data were overlaid over these points to ensure that there was a QLCS and attendant mesocyclone or TVS capable of producing a tornado passing over the points within an hour of the Storm Data reported time. If this did not occur, the event was rejected. If the condition was met, the next step was to correct the tornado starting and ending times based on the timing of the radar data. Specifically, corrections were made by inspecting Storm Relative Motion (SRM) data at the 0.5 degree elevation slice to find those inbound/outbound velocity couplets most likely associated with the tornado. I then interpolated the tornado starting and ending times based on the locations of the Storm Data starting and ending points relative to the position of the couplet. This procedure is shown schematically in Fig. 3.

SRM was estimated by viewing a reflectivity animation of the storm cells. The conversion from V to SRM does not affect the MDA and TDA calculations since the shear and rotational values calculated by these algorithms are not altered when a uniform velocity vector is added.

The only reason for converting V to SRM is to aid the visual determination of where the couplets are located. It is assumed that slight errors in storm motion estimates will have only a negligible impact on the assessment of these couplets.

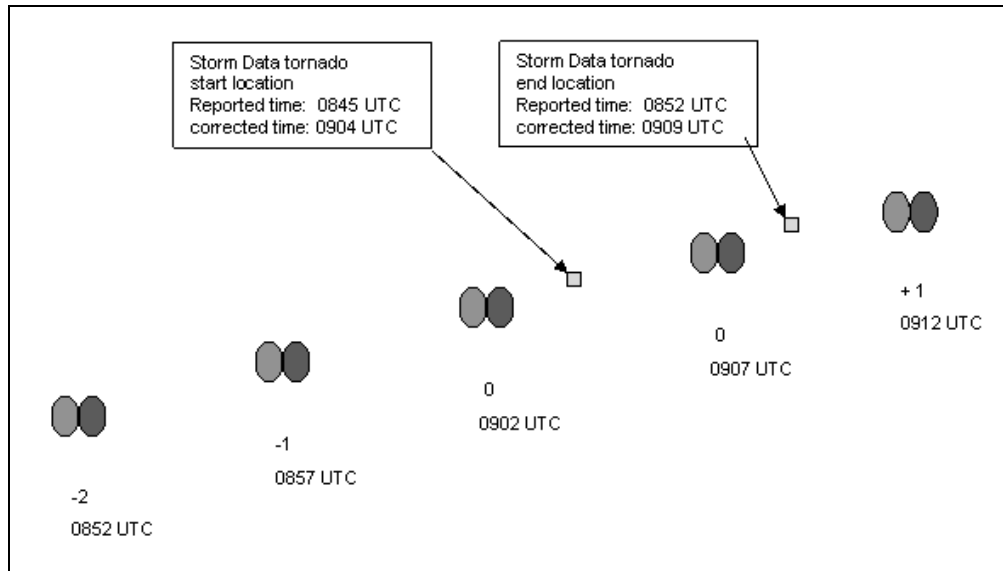


Fig. 3. Time correction of tornado starting and ending locations. The shaded ovals represent the 0.5 degree elevation SRM inbound /outbound couplet for a sequence of volume scans. The first number below each couplet is the scan number relative to the tornado start or end time (0 is during the tornado). Below the scan is the time the velocity data were recorded by the radar.

There were some cases when the Storm Data tornado starting and ending points were identical or very close together, yet a much stronger couplet appeared immediately downstream of the identical points, followed by a much weaker or non-existent couplet in the following scan, as shown schematically in Fig. 4. In such cases, I assumed that the Storm Data locations were slightly erroneous, and the volume scan with the strongest couplet was used as the tornado time. However, in the vast majority of cases, the differences in strength of the mesocyclone or TVS among the scans were negligible; so the Storm Data locations were assumed to be correct.

Once the events for each episode were selected, the mesocyclone and TVS detections that best matched the low-level vortex were collected for each scan during the tornado occurrence, as well as for scans -1 through -4, using the nomenclature in Fig. 3. A possible source of error is that it was not always possible to track a consistent Mesocyclone or TVS circulation this far in advance of the tornado occurrence. One reason for this tracking difficulty is the rapidly developing nature of the non-descending TVSs that are so commonly observed with QLCS tornadoes (Trapp et al. 1999). Another possible source of error is the way the MDA and TDA forecast a future mesocyclone or TVS position based on extrapolation, and then select the actual mesocyclone or TVS in the following scan that is closest to the predicted location. If there

is non-linear motion or a significant change in speed, as occurs during a mesocyclone occlusion, the true continuity can be lost since the low-level circulation is erroneously assigned a new Mesocyclone or TVS identifier (e.g., see Turnage 2001). When this occurred, the best candidate Mesocyclone or TVS was selected from each volume scan.

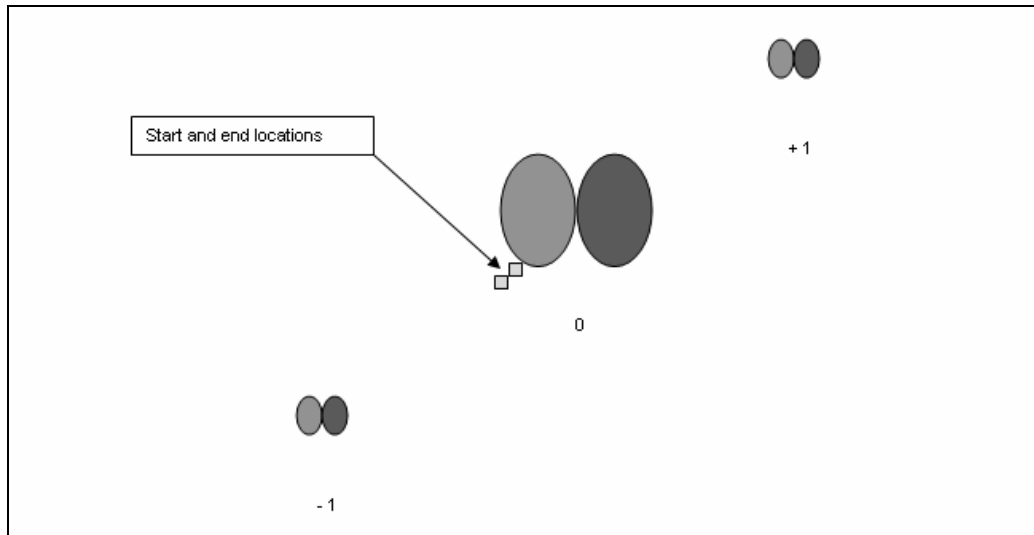


Fig. 4. Time correction for a case when the couplet strengthens significantly, shown schematically by the larger couplet, and then weakens again in the following scan. The Storm Data start and end locations are nearly identical, with the strengthening occurring immediately downstream. In this case, the tornado start and ending times are assumed to be nearly identical and associated with the scan containing the strongest couplet.

Each step of classifying a QLCS episode, correcting the tornado times and determining the mesocyclone/TVS detections associated with the tornado introduces some unavoidable degree of subjectivity. Of the three steps, the matching process undoubtedly is the most subjective. On many occasions, multiple mesocyclone or TVS detections were identified simultaneously in close proximity to the same tornadic velocity couplet. In these cases the mesocyclone or TVS with the most superior rank or largest Strength Index was selected, assuming it was still in a reasonable location relative to the velocity couplet. In addition, as observed by Weisman and Trapp (2003) during simulations of marginal shear QLCS events, an upshear displacement of the mid-level mesocyclone relative to the low-level vortex can add to the uncertainty. Fortunately, in the more strongly sheared cases, there will be a stronger connection between the lower and middle levels, and consequently a greater probability for tornadoes, as vortex stretching is induced in the low-level vortex.

It was important to construct a meaningful null detection dataset to compare with the

tornadic detection dataset, preferably by selecting detections that were spatially and temporally close to the tornadoes. During a tornado episode, a radar volume scan can reveal one or more mesocyclone or TVS detections within its effective range, yet only a fraction of these detections will be associated with a tornado. Those detections not associated with a reported tornado comprised the null set. They were spatially close enough to the tornadoes to yield a meaningful comparison.

Temporal proximity of the null detection dataset was attained by first identifying all detections that occurred in every scan beginning six scans prior to the onset of the first tornado and terminating at the second scan following the end of the last tornado. Once these detections were collected, the tornadic detections were extracted, leaving only the null detections.

To ensure the best possible temporal proximity of null detections to tornadic detections, the scan to event ratio was considered. For example, if an episode contained a single event that lasted one volume scan, there would be a total of 9 scans for that episode:

6 scans (prior to the tornado) + 1 scan (during the tornado) + 2 scans (after the tornado) = 9 scans

This yields a 9:1 scan-to-event ratio. If an episode contained 2 events lasting 2 scans each, and the events were separated by one scan, the result would be 13 scans:

6 scans (prior to tornado 1) + 2 scans (during tornado 1) + 1 scan (between tornadoes) + 2 scans (during tornado 2) + 2 scans (after tornado 2) = 13 scans

This yields a scan-to-event ratio of 13:2.

To ensure a null detection dataset that was temporally close to the tornado detections, the maximum allowable scan-to-event ratio was set to 10:1 or less (Table 2). For the entire dataset the scan-to-event ratio was 455:86, or approximately 5:3. Although eleven of the twenty-two episodes were taken from the M03 dataset, every event was analyzed using the methodology described above.

The null dataset likely includes some detections associated with non-QLCS tornadoes, especially those episodes containing isolated supercells ahead of a QLCS. An example was depicted in Fig. 2, where a possibly tornadic supercell is located in the bottom center of each image ahead of the QLCS. It also is possible that the dataset contains unreported tornadoes. Therefore, it is misleading to call the null detection dataset a false alarm dataset since it is impossible to know with certainty whether a tornado occurred with any given detection. However,

given the large total number of mesocyclone and TVS detections acquired, the unreported tornado detections and non-QLCS tornado detections are assumed to be proportionally very small, and therefore likely to have little adverse influence on the null dataset.

Table 2. Tornado episodes and events.

Date	Radar	Radar location	# scans	# events
1997-02-21	KGSP	Greer SC	14	2
1998-03-08	KCAE	Columbia SC	22	4
1998-03-08	KLTX	Wilmington NC	25	2
1998-06-05	KLZK	Little Rock AR	10	3
1998-06-18	KDVN	Davenport IA	16	2
1998-06-29	KDVN	Davenport IA	18	6
1998-06-29	KILX	Lincoln IL	26	5
1998-11-10	KSRX	Ft. Smith AR	15	2
1999-01-02	KLCH	Lake Charles LA	47	10
1999-01-02	KTLH	Tallahassee FL	9	1
1999-01-22	KSHV	Shreveport LA	13	2
1999-02-11	KLSX	St Louis MO	15	3
1999-02-28	KBMX	Birmingham AL	26	3
2002-12-24	KJAX	Jacksonville FL	30	9
2003-03-06	KHTX	Huntsville AL	9	1
2003-03-20	KTLH	Tallahassee FL	26	2
2003-05-17	KHTX	Huntsville AL	11	1
2003-06-10	KLSX	St Louis MO	19	7
2004-11-24	KBMX	Birmingham AL	39	11
2004-12-07	KDGX	Jackson MS	23	5
2004-12-07	KGWX	Columbus MS	32	4
2005-04-06	KDGX	Jackson MS	10	1
Totals:		22 episodes	455	86

Finally, in an effort to quantify the subjectivity discussed above, all detections were ranked by confidence level, following the technique described in M03. Level 3 denotes a very high degree of certainty that the selected mesocyclone or TVS was associated with the tornadic or pre-tornadic circulation. Level 2 refers to a moderate confidence level, while level 1 refers to rather low confidence.

2.3 Cases

Beginning locations of the tornado events in this study are plotted in Fig. 5. Due to radar data availability and Storm Data reports, there are noticeable spatial gaps in the events, particularly near Georgia, Tennessee, and Kentucky. However, as noted by previous studies (e.g., Lee et al. 1998), geographic location should not affect storm behavior, whereas the Near-Storm Environment (NSE) will exert a major influence. The associated WSR-88D locations also

are plotted in Fig. 5. Data from the closest available WSR-88D were used for each event.

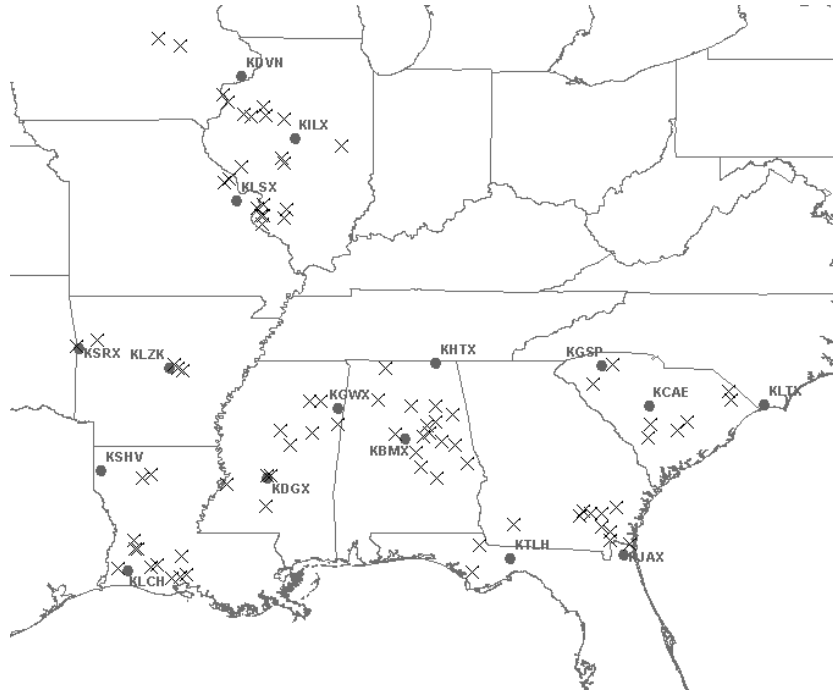


Fig. 5. Tornado event start locations and WSR-88Ds used in the dataset.

The numbers of tornadic versus null detections are displayed in Table 3. It is interesting to note that a much greater percentage of TVS detections (18.7%) are associated with tornadoes, whereas only 4.5% of mesocyclone detections are associated with tornadoes. This agrees with the findings of Stumpf et al. (1998), Jones et al. (2004), and Marzban (2001). The large numbers of mesocyclone and TVS detections lend credence to the assertion that the number of incidental tornadic detections contained within the null detection dataset likely is sufficiently small to have little effect on the results.

Table 3. TVS and mesocyclone detections.

Detections	Tornadic	Null
mesocyclone	330	7384
TVS	100	536

Table 4 gives the number of detections that occur during scans associated with the tornadoes (scan 0), as well as scans 1 through 4 prior to the tornadoes (i.e., scans -1 through -4). The numbers of -3 and -4 TVS detections are too small to be statistically useful. Therefore, the TDA dataset was separated into only three groups: pre-tornadic detections (TPRE), tornadic detections (T0), and the combination of the pretornadic and tornadic detections (TALL). The

mesocyclone detections included all four pre-tornadic scans.

Table 4. Tornadic and pre-tornadic detections before and during tornado occurrences. Numbers in the top row denote the number of scans prior to the tornado, following the convention in Fig. 3 and Fig. 4. Tornado occurrence is denoted by zero.

Detections	Tornado (0)	- 1	- 2	- 3	- 4
mesocyclone	143	66	52	41	28
TVS	55	19	13	7	6

Table 5 shows the distribution of confidence levels assigned to all the mesocyclone or TVS detections associated with an occurring or imminent tornado. Since the number of highly uncertain detections (Confidence = 1) is quite small, they were excluded from the analyses.

Table 5. Distribution of confidence levels assigned to all mesocyclone or TVS detections associated with an occurring or imminent tornado. Numbers in the top row range from 1 (low confidence) to 3 (high confidence).

Confidence	3 (high)	2	1 (low)
mesocyclone / TVS	289	126	15

CHAPTER THREE

RESULTS

3.1 Severe Storms Analysis Package (SSAP) data

Several diagnostic parameters from the operational MDA and TDA were evaluated. Delta Velocity (DV) is a parameter available from both algorithms that is considered to have good predictive value, especially for the TVS (Marzban 2001; also referred to as gate-to-gate velocity difference). DV is defined in the NWS Distance Learning Operations Course for radar (DLOC; 2007) as:

$$DV = \text{Velocity Difference} = \text{Velocity outbound} - \text{Velocity inbound}, \quad (1)$$

where the inbound and outbound velocities must lie on adjacent radar radials and the inbound velocity is conventionally a negative value. DV often is assessed at the lowest level (LLDV), i.e., the lowest WSR-88D elevation slice (Fig. 1). According to the NWS DLOC, a TVS is identified if:

$$DV \geq 45 \text{ m s}^{-1} \text{ and range} < 55.56 \text{ km}, \text{ or}, \quad (2)$$

$$DV \geq 35 \text{ m s}^{-1} \text{ and } 55.56 \text{ km} \leq \text{range} < 101.86 \text{ km}. \quad (3)$$

The Maximum DV (MXDV) of all elevation slices within a mesocyclone or TVS detection also can be measured. Both the MDA and TDA assign a Strength Index (SI) to each mesocyclone/TVS. These are denoted Mesocyclone SI and Tornado SI (MSI and TSI, respectively). The MSI and TSI are calculated by vertically averaging values associated with each 2-dimensional segment comprising the detection.

In addition to measuring DV, the MDA also considers the larger mesocyclone circulation, which often is sampled across several radials. This provides maximum outbound and inbound velocities that are separated by at least one radial, with the associated circulation denoted Rotational Velocity (ROTV). Unlike DV, ROTV uses the average of the magnitudes of the maximum inbound and outbound velocities.

$$\text{ROTV} = (|\text{Max Velocity inbound}| + |\text{Max Velocity outbound}|) / 2 \quad (4)$$

ROTV can be further classified into Low-Level and Maximum values (LLROTV and MXROTV, respectively), where Low-Level refers to the lowest radar elevation slice.

As noted earlier, Manross et al. (2003) determined that Low-Level Convergence (LLCONV) was an effective discriminator between QLCS tornadoes and supercell tornadoes. Stumpf et al. (1998) defines LLCONV as the average radial convergence between 0 and 2 km Above Radar Level (ARL).

Other diagnostic parameters contained within the MDA are Vertically Integrated DV and ROTV (VIDV and VIROTV, respectively). These parameters are additions of DV or ROTV values at each elevation slice of the mesocyclone or TVS. Since both tornadogenesis paradigms involve vertical stretching of strong rotation, one expects that VIDV and VIROTV will increase with time prior to tornadogenesis.

All of the diagnostic parameters described thus far can be grouped into a set of dependent predictor variables that discriminate between tornadic and non-tornadic detections. These parameters, and the algorithm(s) to which they pertain, are summarized in Table 5. The first part of the results investigates the ability of these parameters to discriminate between tornadic and non-tornadic detections.

Table 6. Initial SSAP Predictors used for QLCS tornadoes.

Predictor	MDA or TDA	Base data
LLDV	both	V
MXDV	both	V
HMXDV	both	V
LLROTV	MDA	V
MXROTV	MDA	V
LLCONV	MDA	V
VIDV	MDA	V
VIROTV	MDA	V
VISHR	MDA	V
MSI	MDA	V
TSI	TDA	V

We first examine the diagnostic LLDV (Fig. 6). The most striking difference is between the TVS and Mesocyclone detections. This difference is expected since large DV thresholds must be met for a TVS to be assigned (2 and 3). One should note that many LLDV values are less than the thresholds defined in (2 and 3). This occurs because the requirement for the MDA is not as strict as for the TVS.

Almost as striking (Fig. 6) is the difference between mesocyclone detections during the tornado (M0) and those not associated with an occurring or incipient tornado (Non-Tornadic Mesocyclone; NTM). Values of LLDV gradually increase from three scans prior to the tornado

(M3) through one scan prior to the tornado (M1). Interestingly values of LLDV four scans prior to the tornado (M4) are slightly greater than at 3 scans. It is possible that the relatively small sample of M4 cases introduces a high bias. There is much less difference in LLDV between the TVS detections associated with an occurring or incipient tornado and those not associated with a tornado (Non-Tornadic TVS; NTT). This finding is contrary with those of Marzban (2001). A possible explanation is that Marzban used a more comprehensive tornado dataset that included non-QLCS tornadoes. Nonetheless, the stringent requirements for a TVS and their relative infrequency make it harder to discriminate between QLCS and non-QLCS tornadic cases.

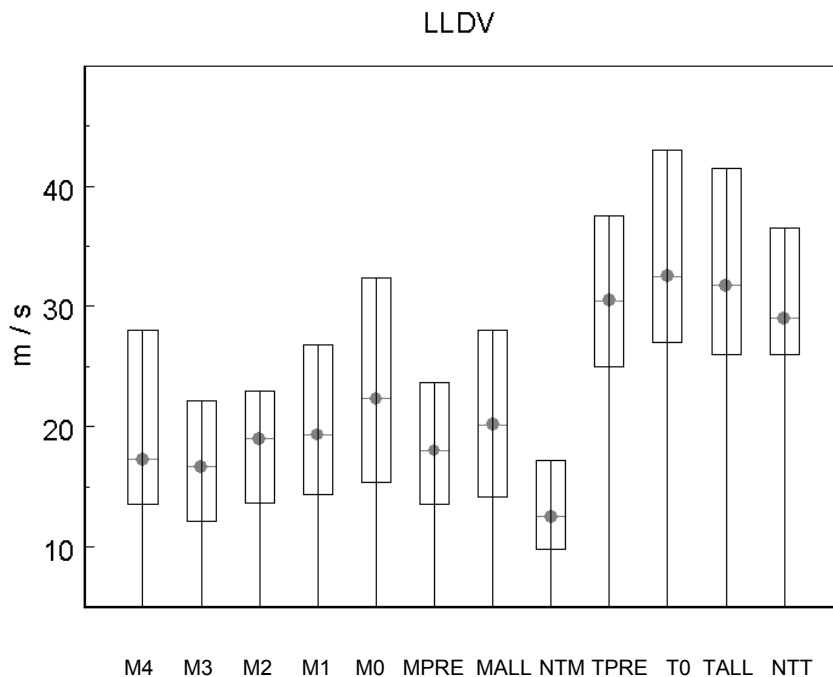


Fig. 6. LLDV quartile box plots. MALL is all mesocyclones during and up to 4 volume scans prior to the QLCS tornadoes. M0 is all mesocyclones during the tornado. M1 through M4 are mesocyclones occurring during volume scans 1 through 4 prior to the tornado. MPRE is the collection of pre-tornado mesocyclones for scans 1 through 4. Non-tornadic mesocyclones comprising the null set are denoted by NTM. TPRE, T0, TALL, and NTT are similarly denoted, except for TVS detections.

Fig. 7 shows the same comparisons, but for the Strength Index (SI; see Stumpf et al. 1998 and Mitchell et al. 1998 regarding the calculation of SI in the Mesocyclone and Tornado Detection Algorithms). Compared to LLDV (Fig. 6), there is much better separation between the tornadic and non-tornadic mesocyclone detections, similar to the findings of Marzban (2001). However, there is less distinction between the tornadic and non-tornadic TVS detections, possibly because values of TSI tend to be smaller than values of MSI.

Results for Low-Level Rotational Velocity (LLROTV) are shown in Fig. 8. LLROTV is not calculated in the Tornado Detection Algorithm (Table 6), resulting in fewer box plots. As with SI

(Fig. 7), there is a pronounced difference between the tornadic and non-tornadic mesocyclone detections, especially when considering only M0. There also is a substantial increase between M1 and M0, as observed with LLDV. To summarize, Fig. 7 and 8 suggest that SI and LLROTV exhibit some skill at differentiating between tornadic and non-tornadic mesocyclone detections.

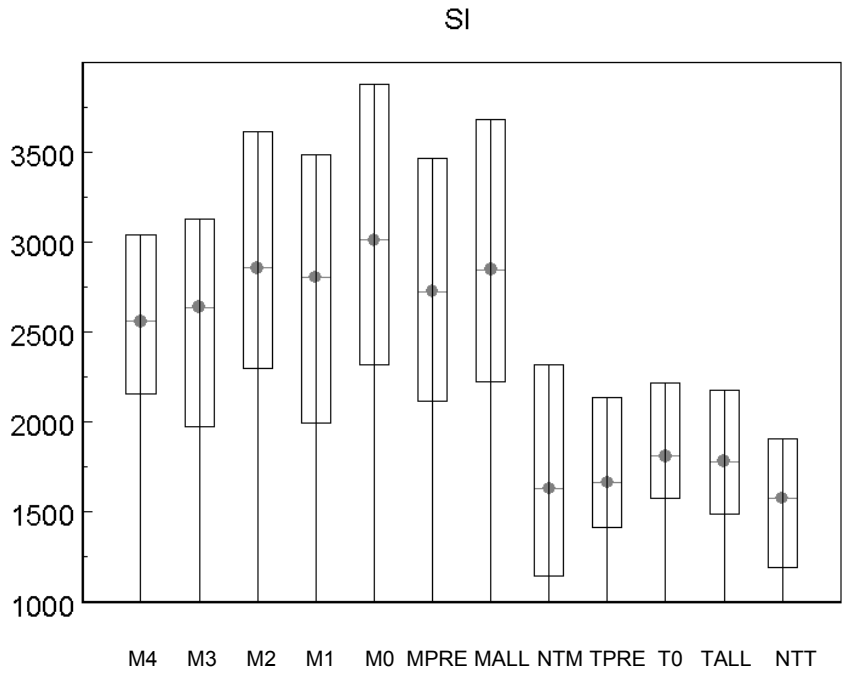


Fig. 7. As in Fig. 6, except for Strength Index. Units are dimensionless.

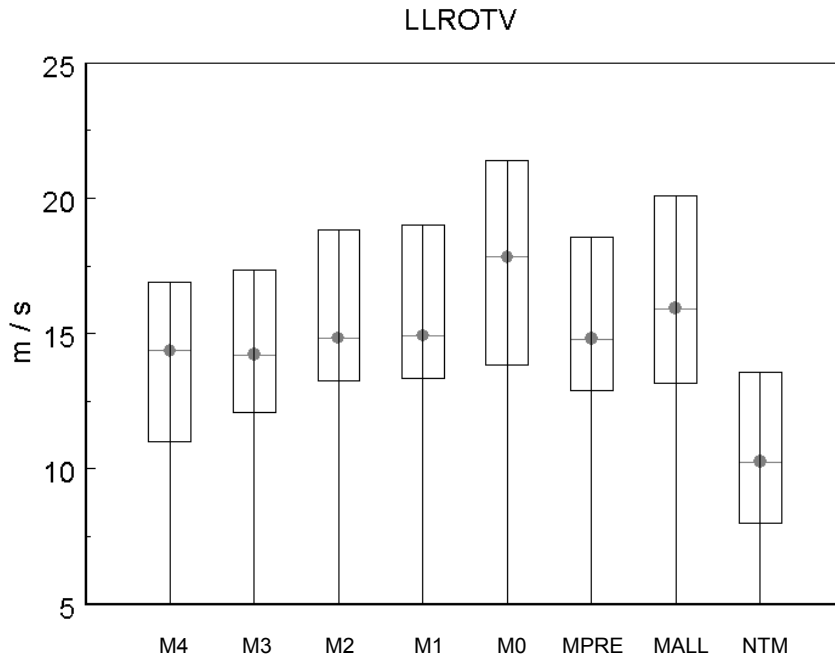


Fig. 8. As in Fig. 6, except for LLROTV. Note the smaller velocity scale. Since TDA LLROTV diagnostics do not exist, they could not be included.

Most of the other diagnostics in Table 6 do not show such pronounced differentiation, and therefore little potential for better prediction. For example, Low-Level Convergence (LLCONV), which M03 found to be an effective discriminator between QLCS tornadoes and supercell tornadoes, is plotted in Fig. 9. Compared to LLROTV (Fig. 8) there is significant overlap between the 50%-75% quartile of the non-tornadic data and the 25%-50% quartile of the tornadic data. This indicates that LLCONV by itself has limited value in discriminating between tornadic and non-tornadic detections. A similar overlap is seen for parameters such as MXROTV, MXDV, VIROTV, and VIDV (not shown), again implying limited utility when used by themselves.

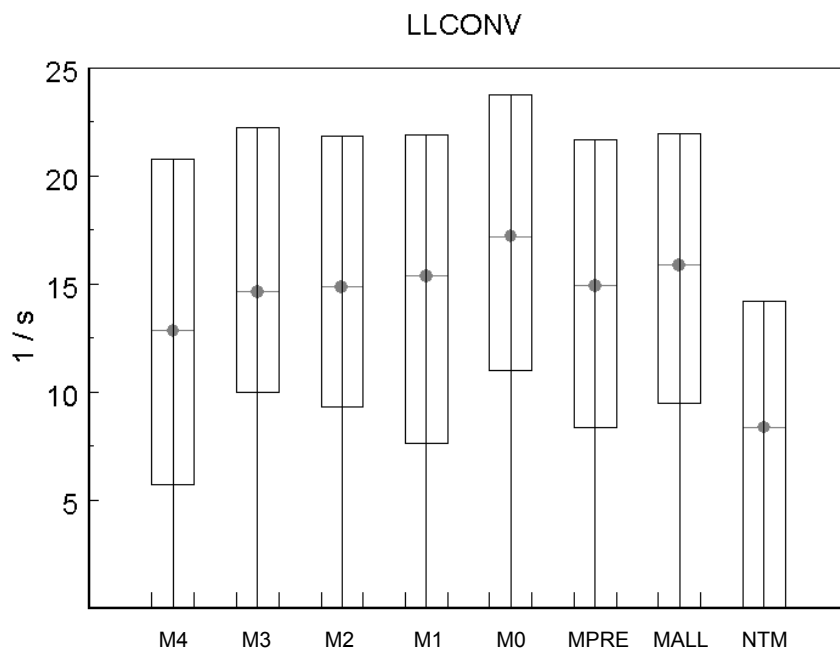


Fig. 9. As in Fig. 6, except for LLCONV.

If most tornadoes follow the non-descending paradigm, the model simulations by Trapp and Davies-Jones (1997) indicate that maximum values of ROTV and DV should remain in the lowest elevation slice of the sampled mesocyclone prior to the onset of the tornado and during tornado occurrence. This would yield a strong correlation between LLROTV and MXROTV, and also between LLDV and MXDV. Fig. 10 shows a correlation matrix between LLDV, MXDV, LLROTV, and MXROTV during scans when tornadoes are occurring, with the associated correlation coefficients listed in Table 7. Results show the expected strong correlation of 0.918 between LLDV and MXDV, while there is a somewhat weaker correlation (0.851) between LLROTV and MXROTV. There are relatively few detections where $LLDV < MXDV$ and $LLROTV < MXROTV$. By definition, no detections exist on the opposite side of this line. Based on (1 and 4), a perfect correlation would be the line defined by $DV = 2 \times ROTV$. However, the points in Fig.

10 actually are distributed on either side of this line, since ROTV and DV are calculated independently. It also is possible for strong mesocyclones to be broad enough to be sampled through many radar radials, possibly yielding large maximum inbound and outbound values, but much smaller values of DV across adjacent radials.

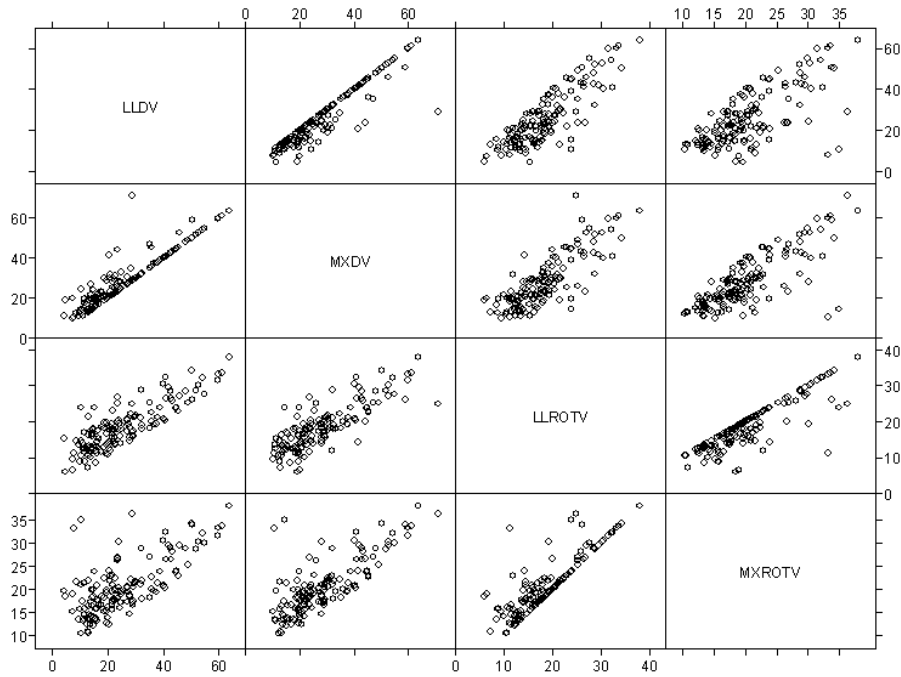


Fig. 10. Scatter plot matrix for Mesocyclone LLDV, MXDV, LLROTV, and MXROTV during tornado occurrence (M0). All units in m s^{-1} .

Table 7. Correlation coefficients for the M0 matrix in Fig. 10.

M0.LLDV	0.918	0.843	0.691
	M0.MXDV	0.810	0.775
		M0.LLROTV	0.851
			M0.MXROTV

Conversely, strong and well-sampled gate-to-gate shear sometimes occurs within weak or poorly sampled mesocyclones. These possibilities could account for the more symmetrical scatter seen in these plots. Thus, the scatter in the data does not necessarily disprove the assertion that QLCS tornadoes follow the non-descending paradigm.

Either tornadogenesis paradigm can explain the finding that strongest circulations occur in the lowest elevation slice during tornado events (Fig. 10). Therefore, it is informative to correlate maximum parameter values with low-level values during the pre-tornadic scans to

determine whether the strongest circulations remain in the lowest levels according to the non-descending mode of tornadogenesis (Trapp et al. 1999). Fig. 11 shows scatter plots for the pre-tornadic mesocyclones, with corresponding correlation coefficients listed in Table 8. When compared to Fig. 10, there are fewer cases when low-level values equal maximum values. Nonetheless, there still are fairly strong correlations between LLDV and MDV (0.803) and between LLROTV and MXROTV (0.742). This tendency for the strongest rotation to remain in the lowest levels prior to the tornado agrees with the non-descending paradigm described by Trapp et al. (1999).

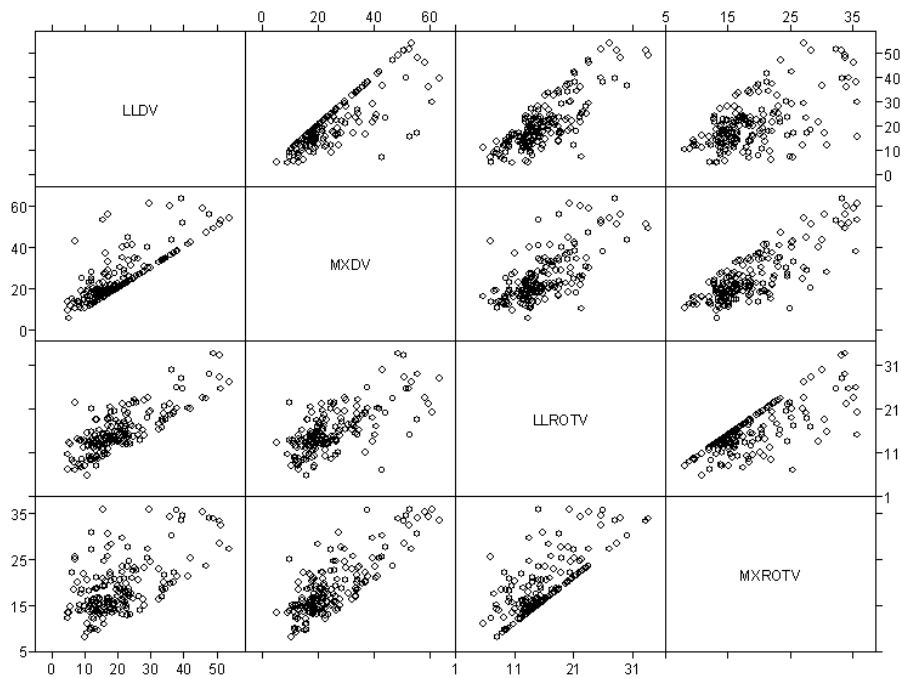


Fig. 11. As in Fig. 10, except prior to tornado occurrence (MPRE).

Table 8. As in Table 7, except for the MPRE matrix in Fig. 11.

MPRE.LLDV	0.803	0.799	0.581
	MPRE.MXDV	0.678	0.805
		MPRE.LLROTV	0.742
			MPRE.MXROTV

3.2 Regression Tree Models

The previous section indicated that some SSAP diagnostics exhibit predictive skill when used individually; however, other parameters showed little skill. The next step is to determine whether combinations of diagnostics can increase the predictive skill. Marzban et al. (1999) noted that a strong correlation between predictors (as seen in Table 7) introduces the possibility of co-linear interactions between predictors, precluding the creation of a meaningful multivariate statistical model. They stressed that bivariate analysis (where one predictor is analyzed at a time) is not adversely affected by the unpredictable interactions that can arise between strongly correlated predictors.

To examine the concerns of Marzban et al., I first calculated correlations among the parameters (Table 6) and placed results for the Mesocyclone Detection Algorithm (MDA) into a correlation coefficient matrix (Table 9). Numbers above the gray diagonal are coefficients among the SSAP parameters between the mesocyclone detections not associated with an occurring or imminent tornado (NTM) and the mesocyclone detections associated with an occurring tornado (M0). Numbers below the gray diagonal are coefficients between the NTM and pre-tornadic (MPRE) detections. Thus, there are differences between values above and below the diagonal.

The Mesocyclone Strength Index (MSI) is the vertical integration of strength ranks at each radar elevation slice (Fig. 1; Stumpf et al. 1998). These ranks are derived from the magnitudes of Delta Velocity (DV), Rotational Velocity (ROTV), or Shear (SHR) at each elevation slice. Therefore, one expects strong correlations between MSI and the vertically integrated values of these individual diagnostics (i.e., VIDV, VIROTV, and VISHR). Table 9 shows that the largest correlation is between MSI and VIRTOTV followed by MXDV and VIDV.

Section 3.1 discussed the non-descending tornadogenesis paradigm which predicts strong correlation between MXDV and LLDV and between LLROTV and MXROTV. This was observed in Table 7 and Table 8, and appears again in Table 9. Similarly, the Tornado Strength Index (TSI) is based entirely on the vertical integration of DV (Mitchell et al. 1998). Although we expect a large correlation between TSI and VIDV, VIDV unfortunately is not available from the TDA. Table 10 is the correlation coefficient matrix for the available TDA diagnostics. Coefficients above the gray diagonal represent the non-tornadic TVS detections (NTT) versus detections associated with an occurring tornado (T0), while values below the diagonal are for NTT versus pre-tornadic detections (TPRE). None of the correlations is particularly large, which is fortunate since only a small number of TDA diagnostics is available to combine.

By accounting for the characteristics of the MSI and TSI diagnostics and using a correlation coefficient of 0.70 as a limiting value, the diagnostics listed in Table 6 were refined into

a subset of MDA and TDA SSAP parameters that should be least likely to exhibit co-linearity (Table 11). MSI was omitted due to its strong dependence on other diagnostics. Since we are presupposing the non-descending mode of tornadogenesis, LLDV and LLROTV were selected instead of MXDV and MXROTV.

Table 9. Correlation coefficients for the MDA SSAP parameters listed in Table 6. Coefficients above the gray diagonal are for the non-tornadic mesocyclone detection (NTM) versus tornadic mesocyclone detection (M0) datasets. Coefficients below the diagonal are for the NTM versus pre-tornadic mesocyclone detection (MPRE) datasets.

	LLDV	MXDV	HMXDV	MSI	LLROTV	MXROTV	VIDV	VIROTV	VISHR	LLCONV
LLDV		0.77	-0.24	0.55	0.79	0.53	0.77	0.41	0.27	0.15
MXDV	0.76		-0.01	0.62	0.65	0.78	0.86	0.54	0.31	0.19
HMXDV	-0.23	-0.00		-0.17	-0.29	-0.06	-0.04	-0.09	-0.11	-0.33
MSI	0.54	0.62	-0.16		0.71	0.74	0.75	0.93	0.64	0.33
LLROTV	0.79	0.64	-0.29	0.70		0.72	0.65	0.63	0.29	0.33
MXROTV	0.52	0.78	-0.05	0.74	0.71		0.67	0.76	0.32	0.35
VIDV	0.77	0.86	-0.03	0.75	0.65	0.67		0.69	0.45	0.20
VIROTV	0.40	0.53	-0.08	0.93	0.62	0.76	0.69		0.65	0.38
VISHR	0.26	0.31	-0.10	0.64	0.29	0.32	0.45	0.65		0.26
LLCONV	0.12	0.17	-0.32	0.33	0.32	0.34	0.19	0.38	0.26	

Table 10. As in Table 9, except for the TDA SSAP parameters. The comparison above the gray diagonal is for non-tornadic TVS detections (NTT) versus tornadic TVS detections (T0) and below the diagonal is NTT versus pre-tornadic TVS detections (TPRE).

	LLDV	MXDV	HMXDV	TSI
LLDV		0.56	-0.33	0.42
MXDV	0.53		-0.04	0.60
HMXDV	-0.31	-0.00		-0.49
TSI	0.39	0.59	-0.47	

The regression tree model is a powerful method for evaluating combinations of predictors (Brieman et al. 1984). As discussed in Crawley (2002), tree models are an excellent tool for initial data inspection, and they give insights into the kinds of interactions that occur between variables. Crawley also explains how a tree model is interpreted. Starting at the top of the tree (misleadingly called the “root”), a path is traced to a terminal node at the bottom of the tree by following a succession of rules (known as “splits”). The variables with the greatest explanatory power are selected first, with a threshold value chosen to give the smallest deviance between the split datasets. A large number of nodes increases the risk of over-fitting the dataset and reduces the ability of the model to generalize to independent datasets (Venables and Ripley 1997).

Therefore, it is wise to “prune” the tree to a limited number of terminal nodes. Cross validation can be used to determine the number of nodes at which over-fitting is likely to begin.

Table 11. Modified list of SSAP diagnostics. Yes or No indicates whether the diagnostic was used for regression trees. NA means the diagnostic is not available.

Predictor	MDA	TDA
LLDV	Yes	Yes
MXDV	No	Yes
HMXDV	Yes	Yes
LLROTV	No	NA
MXROTV	No	NA
LLCONV	Yes	NA
VIDV	No	NA
VIROTV	Yes	NA
VISHR	Yes	NA
MSI	No	NA
TSI	NA	Yes

I determined the optimum number of terminal nodes by applying 10-fold cross validation to a variety of comparative datasets to establish how deviance increases with increasing numbers of nodes. Comparisons for non-tornadic mesocyclones (NTM) versus mesocyclones associated with an occurring tornado (M0) and non-tornadic TVSSs (NTT) versus TVSSs associated with an occurring tornado (T0; Fig. 12 and Fig. 13, respectively) typify the results obtained from other comparisons (not shown). Fig. 6 indicated that these particular comparisons should exhibit the largest qualitative differences. Fig. 12 reveals that deviance among the cross-validation members begins to increase significantly for regression trees containing more than six nodes. In Fig. 13, the increase in deviance occurs earlier, at four nodes. This means that regression trees containing more than six terminal nodes are less likely to apply to independent datasets, although the problem is possible with more than four nodes. Based on these results, I limited the size of the regression trees to four nodes.

Using the tree sizes discussed above and the modified list of SSAP predictors (Table 11), I first differentiated between Non-Tornadic Mesocyclone (NTM) detections and the subset of tornadic detections where a tornado is occurring (M0; Fig. 14). The most explanatory diagnostic is VIROTV with a threshold of 11.0 m s^{-1} . The split is interpreted as follows: When $\text{VIROTV} < 11.0 \text{ m s}^{-1}$ (denoted by “T” for True), there is a 0.9% success rate for identifying an M0 detection. If $\text{VIROTV} \geq 11.0 \text{ m s}^{-1}$ (denoted by “F” for False), the next strongest parameter to investigate is LLDV. If $\text{LLDV} < 19.6 \text{ m s}^{-1}$, there is a 3.2% success rate for identifying an M0 detection. If $\text{LLDV} \geq 19.6 \text{ m s}^{-1}$, LLCONV is the next strongest parameter to investigate. If thresholds for VIROTV, LLDV, and LLCONV are met or exceeded, there is a 28.1% success rate for identifying an M0 detection. If only the first two thresholds are met or exceeded, there is still a 9.7% success rate.

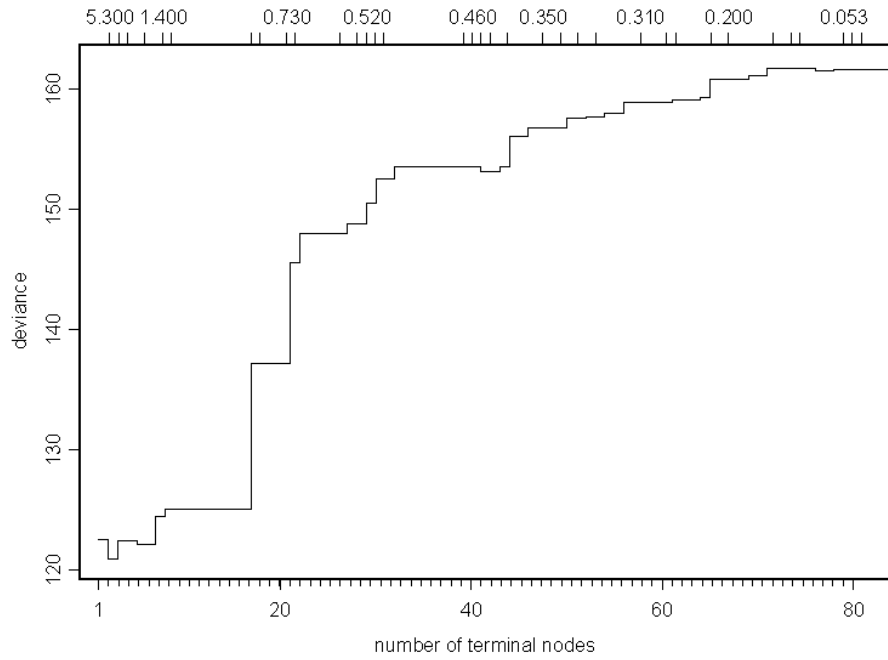


Fig. 12. Deviance measured from a 10-fold cross validation of the NTM versus M0 regression tree.

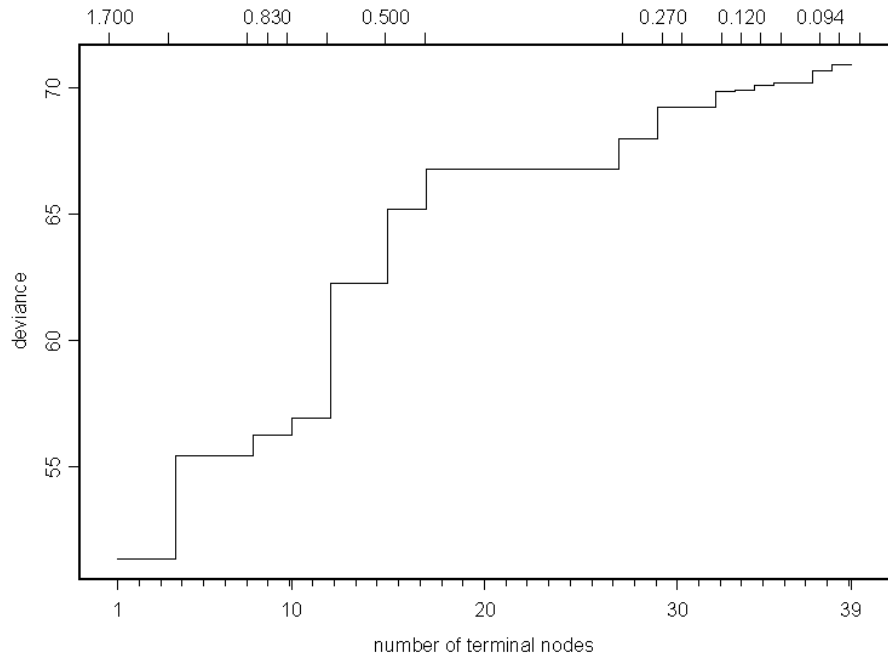


Fig. 13. As in Fig. 12, except for the NTT versus T0 regression tree.

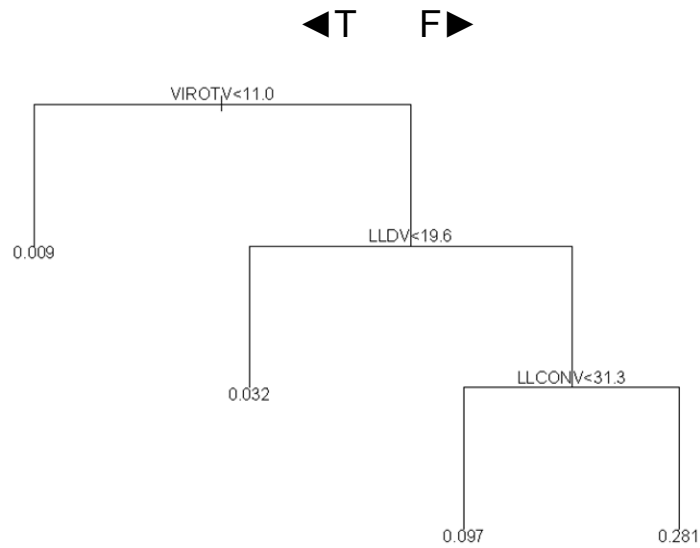


Fig. 14. Regression tree for Non-Tornadic Mesocyclone (NTM) versus Mesocyclone detections during tornado occurrence (M0). In this case, Vertically Integrated Rotational Velocity (VIROTV) is the parameter best able to discriminate between the NTM and M0 datasets. If $VIROTV < 11.0 \text{ m s}^{-1}$, there is a 0.9% percent chance of the detection being an M0 detection. If $VIROTV \geq 11.0 \text{ m s}^{-1}$, then Low-Level Delta Velocity (LLDV) is the next most effective parameter to discriminate between the datasets. The number at the end of each branch denotes the ratio of M0 detections for the set of conditions leading to the branch.

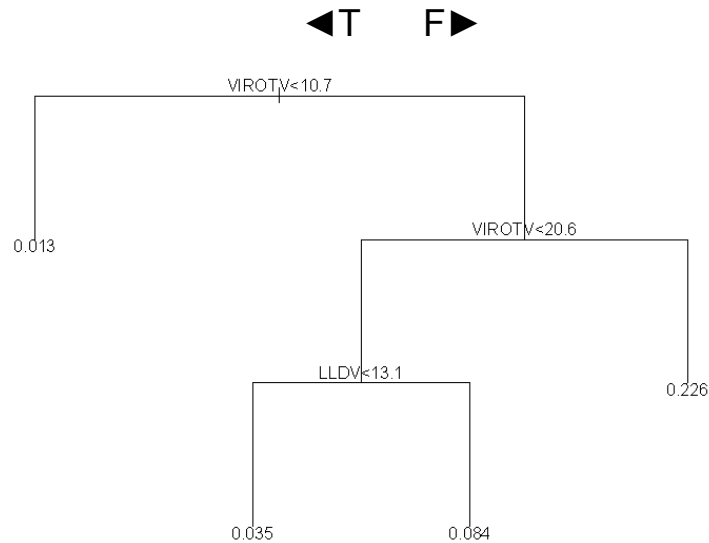


Fig. 15. Regression tree with 4 terminal nodes for NTM versus MPRE detections.

We next compare NTM detections with pre-tornadic mesocyclone detections (MPRE; Fig. 15). Four terminal nodes were chosen because of the redundancy in predictors that occurs with six nodes (not shown). The parameters selected for this tree are very similar to those in Fig. 14, with VIROTV again being most important, followed by LLDV. Since VIROTV is a vertically integrated quantity, it is surprising to find it important in MPRE detections because the non-descending paradigm predicts that the depth of strong rotation increases with the onset of the tornado, not prior to its occurrence. It also is interesting that VIROTV appears twice in the regression tree. However, this appearance is sequential, implying that increasing values of VIROTV rapidly increase the success rate of MPRE detection. In this case, increasing VIROTV from $< 10.7 \text{ m s}^{-1}$ to $\geq 20.6 \text{ m s}^{-1}$ increases the success rate from 1.3% to 22.6%. An intermediate parameter occurring between the VIROTV selections would suggest non-linear interactions among the parameters. Assuming that LLDV falls between 10.7 and 20.6 m s^{-1} , LLDV can be used as a third parameter, but the success rates are smaller than if $\text{LLDV} \geq 20.6 \text{ m s}^{-1}$.

A regression tree discriminating between NTM and MALL detections is presented last (Fig. 16). As in Fig. 14 and Fig. 15, VIROTV and LLDV are the dominant predictors, with a 17.1% success rate if the specified criteria are met or exceeded. Although HMXDV appears in another branch, the MALL detection success rates are small regardless of the actual HMXDV value. It is encouraging that Fig. 14 -Fig. 16 contain the same predictors. This lessens the concern that the regression trees are over-fitting the datasets.

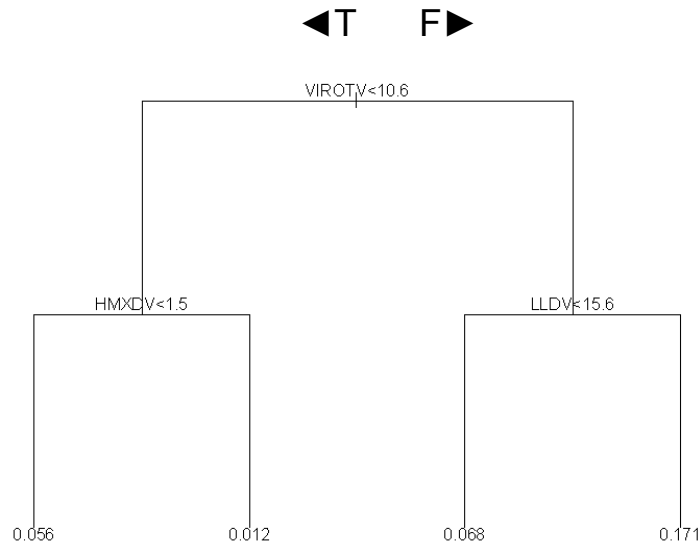


Fig. 16. Regression tree for NTM versus MALL detections.

We next consider the TDA, recalling that there are fewer available predictors compared to the MDA (Table 6). The first tree is for Non-Tornadic TVS (NTT) versus tornadic TVS (T0) detections (Fig. 17). The most important diagnostic is the Height of MXDV (HMXDV). There is less than a 5% chance of aT0 detection if MXDV occurs at a height greater than 2.3 km. This implies that MXDV must be in the lowest elevation slice for mesocyclone detection (Fig. 10). It also implies that a storm must be very near the radar. Specifically, using the standard refractive conditions discussed in NWS DLOC, a radar beam centerline height of 2.4 km corresponds to a range of ~35 km (only 19 n mi.)! This implies a low probability of detecting a tornadic TVS unless it is very near the radar. However, if the small HMXDV threshold is met, then the probabilities of having successful T0 detections are 31.3% and 36.6%, respectively. Unfortunately, these values likely yield a small POD since there is only a small probability that T0 detections will occur so close to a radar.

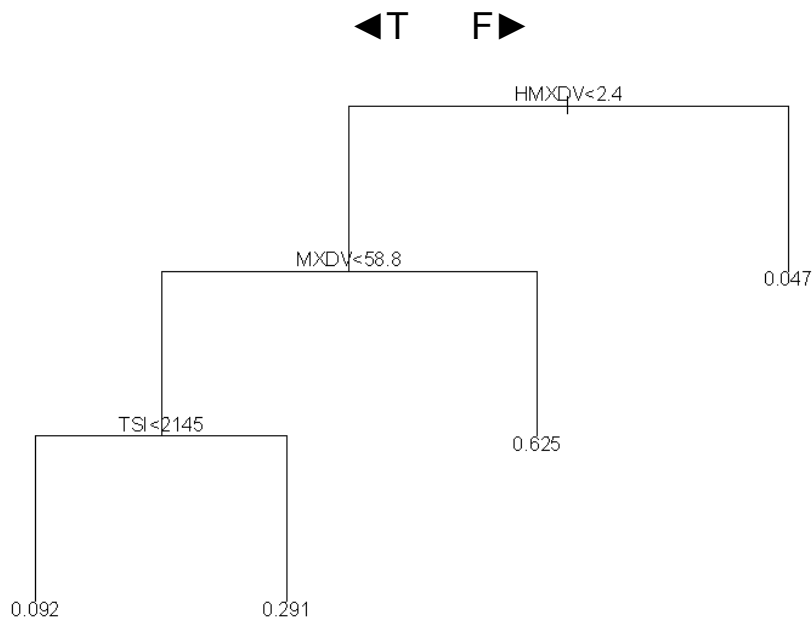


Fig. 17. Regression tree for NTT versus T0 detections.

Fig. 18 shows the regression tree for NTT versus pre-tornadic TVS (TPRE) detections. TSI is the dominant predictor. However, the next split is suspicious since it indicates a better success rate for TPRE detections (28.6%) when $HMXDV \geq 6.15$ km. This contradicts the close range requirement stipulated in Fig. 17. This contradiction may be the result of over-fitting the smaller TVS dataset and the smaller number of available TDA predictors. Regardless of the cause, it is worth noting that TSI and HMXDV are the dominant predictors (Fig. 17 and Fig. 18).

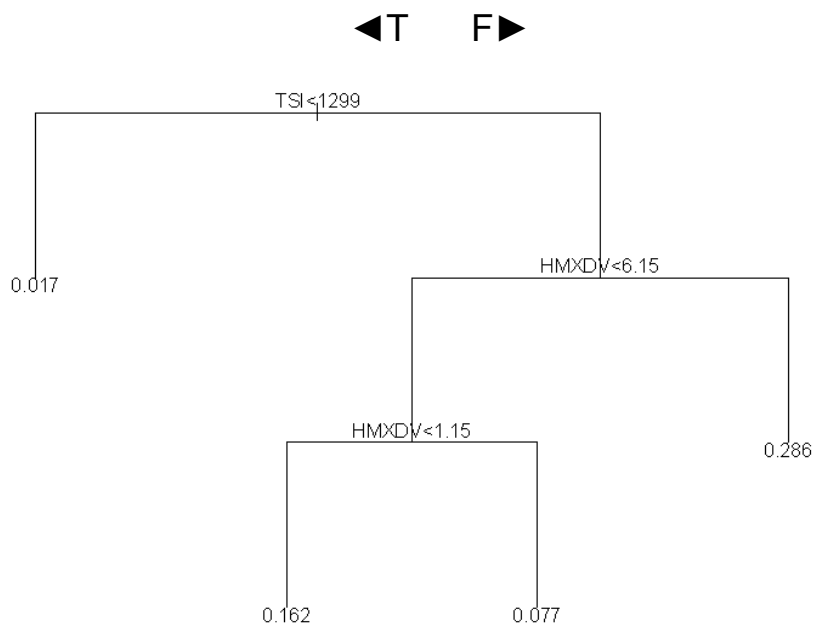


Fig. 18. Regression tree for NTT versus TPRES detections.

Regression trees were investigated to determine whether combinations of predictors were better able than individual parameters to discriminate between tornadic and non-tornadic detections of mesocyclones or TVSS. It is encouraging to see a recurrence of certain predictors since this suggests that the trees were sufficiently pruned to produce similar results that generalize to different datasets. It also is encouraging to observe success rates exceeding 30% for some combinations of predictors.

To test whether combinations of predictors yield greater success rates, I recalculated the regression trees in Fig. 14 and Fig. 17 using only the parameter that appeared at the first split of each tree. The best success rates from the resulting single node trees are 15.9% and 14.9%, respectively (not shown). These values are considerably smaller than the 28.1% and 62.5% success rates observed in Fig. 14 and Fig. 17. In these cases, a combination of predictors does yield greater success rates; however, this improvement is not observed with all possible regression trees (not shown).

3.3 Additional parameters

Up to this point we have investigated only diagnostic parameters that are operationally available to NWS forecasters through the MDA and TDA and which rely exclusively on base velocity (V). We next investigate three new products: Spectrum Width (SW), Reflectivity Variance (REV), and Azimuthal Shear (AZ) to determine whether they can be combined with the MDA or TDA to improve the ability of these algorithms to discriminate between tornadic and non-tornadic QLCS circulations.

SW is a base product that can be displayed operationally in real-time, although there currently is no way to correlate SW values with locations of mesocyclones and TVS detections except through visual comparisons which are subjective and difficult to replicate. Reflectivity is another base product that can be displayed in near real-time, but since REV must be computed, it is not operationally available. AZ also is operationally unavailable, and is calculated exclusively from V. However, instead of calculating shear segments (Stumpf et al. 1998; Mitchell et al. 1998), AZ is based on linear least squares derivatives (Smith et al. 2003).

None of these three products can be mapped to MDA or TDA output in a methodical, precise, or replicable manner since neither operational algorithm considers the measurements. To overcome this problem, I used the Warning Decision Support System - Information Integration (WDSSII) Application Programming Interface (API) described by Lakshmanan (2002) to create applications that calculate Azimuthal Shear and Reflectivity Variance and extract data from the Spectrum Width product. Specifically, the applications were designed to:

- 1) Identify the centroid location of every mesocyclone and TVS detection.
- 2) Convert the centroid location into an azimuth and range from the WSR-88D being interrogated.
- 3) Extract the Reflectivity or SW data array centered at the azimuth and range from the radar within the lowest elevation slice. AZ also would be calculated from V within this array.
- 4) Calculate the mean or variance of the extracted or calculated data array. And finally,
- 5) Append the result to a data table containing the other diagnostic parameters for every detection.

Fig. 19 is a schematic of the data extraction process. The view is from above, with the WSR-88D at the bottom of the figure. The columns depict adjacent radials in the lowest elevation slice (0.5 degrees; Fig. 1), while the range increments (“gates”) are denoted by rows. Each box represents a data “bin” that contains a single value of Reflectivity, Velocity, or Spectrum Width. These bins are at the native resolution of the radar, which exceeds what is operationally available (Table 1), and contrary to what is implied by Fig. 19 the bins become larger with increasing range from the radar due to beam spreading. The dark center bin containing the “X” Fig. 19 denotes the horizontal position of a Mesocyclone or a TVS 3-dimensional centroid. The centroid bin and the surrounding lighter shaded bins represent a data array. Using the WDSSII API, one can calculate the mean and variance at the centroid bin by defining 2-dimensional data arrays such as these.

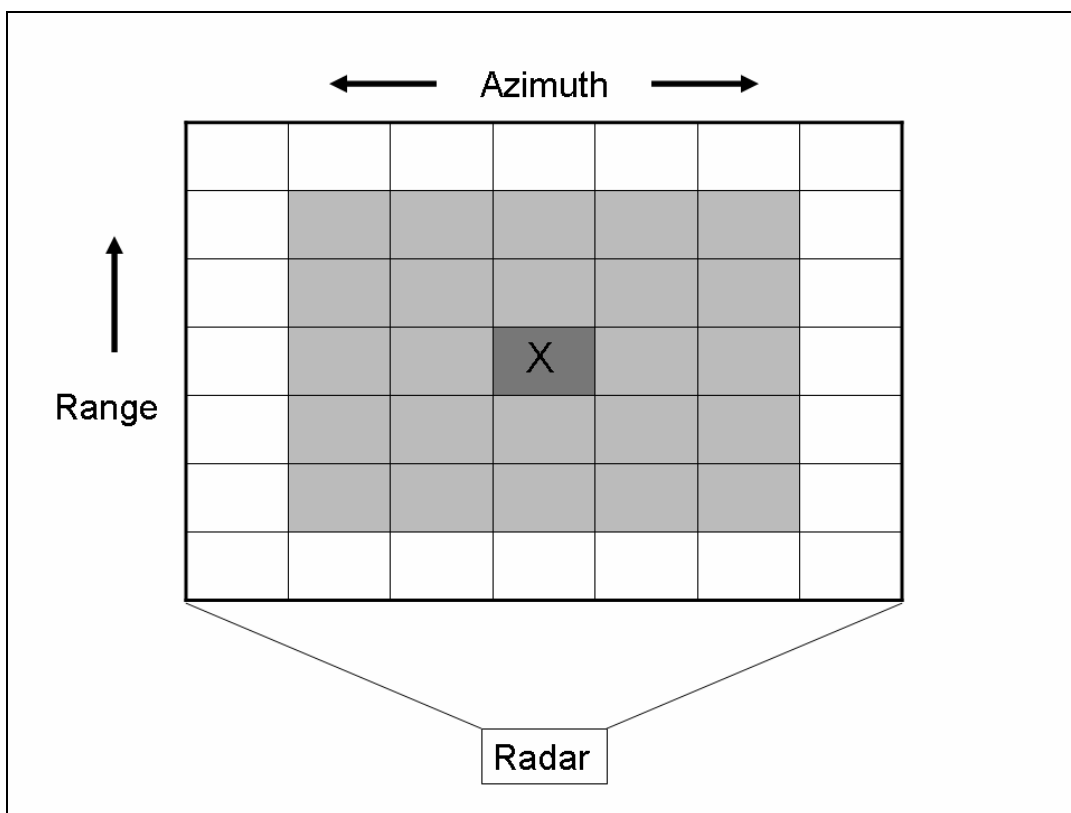


Fig. 19. Schematic of a data array. The dark box marked by an “X” corresponds to the range gate and azimuth associated with the centroid of the detection. The centroid plus the lighter shaded boxes represent the area over which means and variances are calculated for the centroid location. This particular example represents a 5 X 5 array, i.e., an array size of 5.

I investigated array sizes of 1, 3, 5, 7, 9, and 11(see Fig. 19 for an explanation). The arrays that ultimately were chosen are listed in Table 12. The larger SW arrays were examined with the hope they would mitigate noise associated with SW data. Since AZ is based on a linear least squares derivative which smooths the V data, the mean of the array seemed more meaningful than its variance. Finally, the local gradient of Reflectivity was considered more

important than its magnitude. The former could be inferred through variance, although large variance also could be due to noisy data instead of an organized gradient.

Individual centroid bin values of SW and AZ also are included in Table 12 (i.e., array size = 1). However, due to the way that local means and variances are calculated in the WDSSII API an array size of 3 produces the same value as an array size of 1. Therefore, array sizes of 3 were omitted. Results show that certain array statistics are more important than others. For example, the local variance of Reflectivity at the detection centroid (RE#V, where # is the size of the array) was considered more important than the local mean. Also, since AZ already is computed in a manner similar to variance, computing AZ#V gives little additional useful information.

Table 12. Additional non-SSAP parameters.

Product	Base data	Array property	Array sizes	Symbol
SW	SW	mean	1,5,7,9,11	SW, SW5, SW7, ...
SW	SW	variance	5,7,9,11	SW5V, SW7V, ...
AZ	V	mean	1,5,7	AZ, AZ5, AZ7
REV	RE	variance	5,7,9,11	RE5V, RE7V, ...

It should be emphasized that this part of the study is unique. Previous studies have assessed SSAP parameters for tornado detection (e.g., Marzban 2001; Jones et al. 2004), and M03 did this specifically for QLCS tornadoes. However, to the author’s knowledge, no one has determined whether selected properties of SW, RE, or AZ can discriminate between tornadic and non-tornadic mesocyclone and TVS detections.

3.3.1 Spectrum Width

Spectrum Width (SW) is the first new parameter to consider. We first visually assess the normality of SW measurements using probability distribution histograms. The NTM, MALL, and NTT distributions of SW appear approximately normal for each array size (Fig. 20 -Fig. 22). However, the TALL distribution appears less normal (Fig. 23), possibly due to the smaller size dataset (Table 3). I used a two-sample Kolmogorov-Smirnov (KS) goodness-of-fit test to determine whether statistically significant differences exist between the tornadic and non-tornadic datasets. This test was chosen because it does not require normality in the sample datasets. Overall, p-values in Table 13 are larger than the 0.05 confidence threshold, suggesting that statistically significant differences do not exist.

Table 13. KS values (top rows) and p-values of confidence (bottom rows) from two-sample Kolmogorov-Smirnov goodness of fit tests for different array sizes of SW. The compared samples are listed in the left column.

	n = 1	n = 5	n = 7	n = 9	n = 11
SWn.NTM / SWn.MALL	0.09 0.03	0.08 0.10	0.08 0.08	0.08 0.09	0.08 0.05
SWn.NTM / SWn.MPRE	0.11 0.05	0.09 0.17	0.08 0.22	0.09 0.14	0.10 0.11
SWn.NTM / SWn.M0	0.07 0.61	0.06 0.77	0.08 0.43	0.09 0.25	0.09 0.25
SWn.NTT / SWn.TALL	0.10 0.41	0.11 0.28	0.12 0.25	0.12 0.25	0.13 0.19
SWn.NTT / SWn.TPRE	0.14 0.49	0.14 0.47	0.09 0.95	0.10 0.87	0.10 0.87
SWn.NTT / SWn.T0	0.13 0.35	0.16 0.18	0.16 0.18	0.16 0.19	0.17 0.14

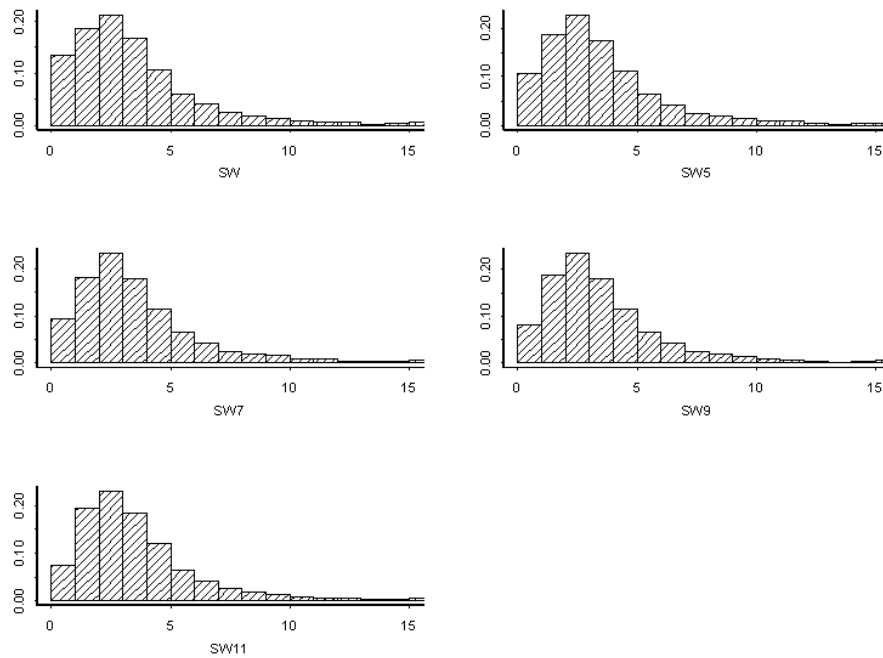


Fig. 20. Probability distribution histograms for the different SW array sizes from the NTM dataset. Units on the abscissa are in $m s^{-1}$.

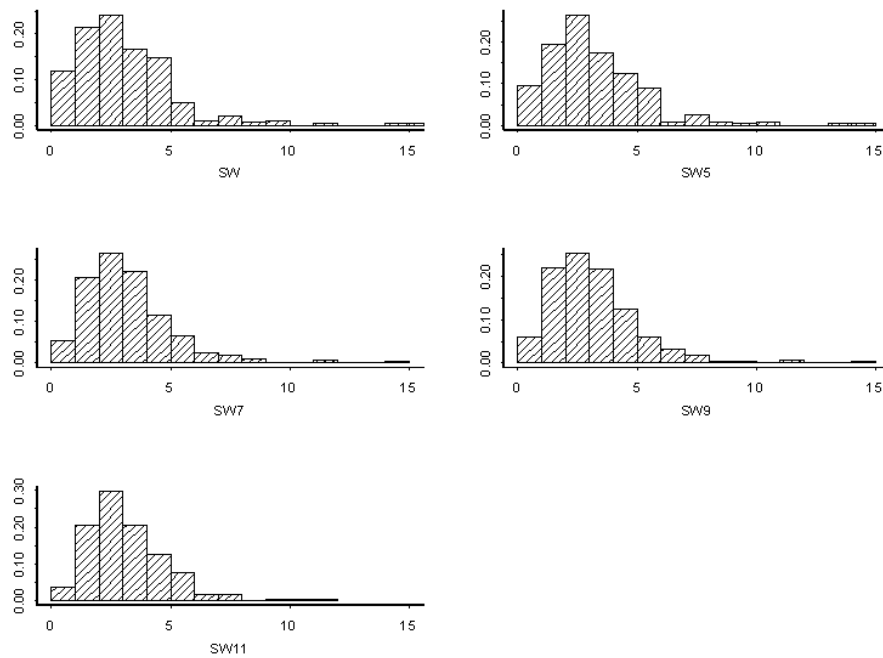


Fig. 21. As in Fig. 20, except from the MALL dataset.

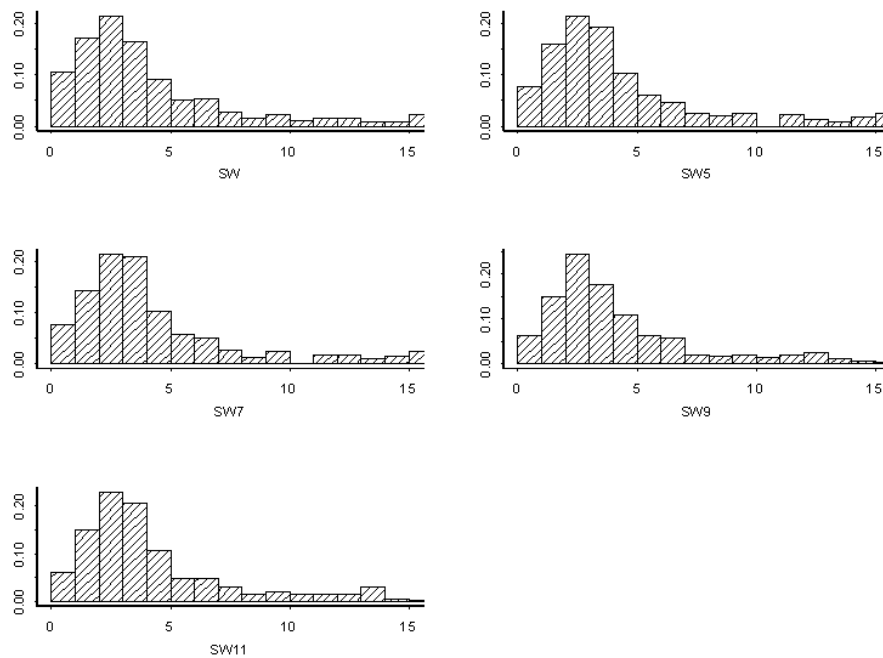


Fig. 22. As in Fig. 20, except from the NTT dataset.

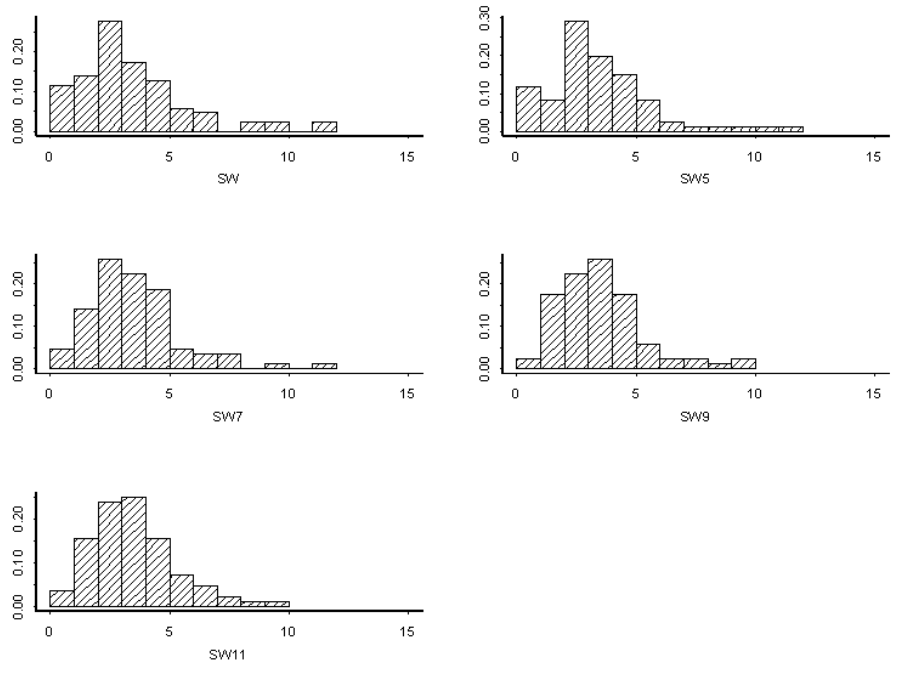


Fig. 23. As in Fig. 20, except from the TALL dataset.

We next utilize box plots to determine whether qualitative differences exist among the different SW datasets, as done previously with the SSAP data. The plots for SW (Fig. 24) are based on the single value at the centroid of each Mesocyclone or TVS detection at the lowest elevation slice (Fig. 19). Among the mesocyclone detections M0, MALL, and NTM, there is no detectable difference. There is a slight increase in the spread of the data between M4 and M1, but this could be due to the large differences in size of these datasets (Table 4). SW values associated with the TVS generally are greater than those of mesocyclone detections, especially for T0 and NTT, but this is not surprising since the TDA is designed to identify strong localized shear (2 and 3; Fig. 6). Strong shear is associated with a large local variance in velocity, resulting in greater SW.

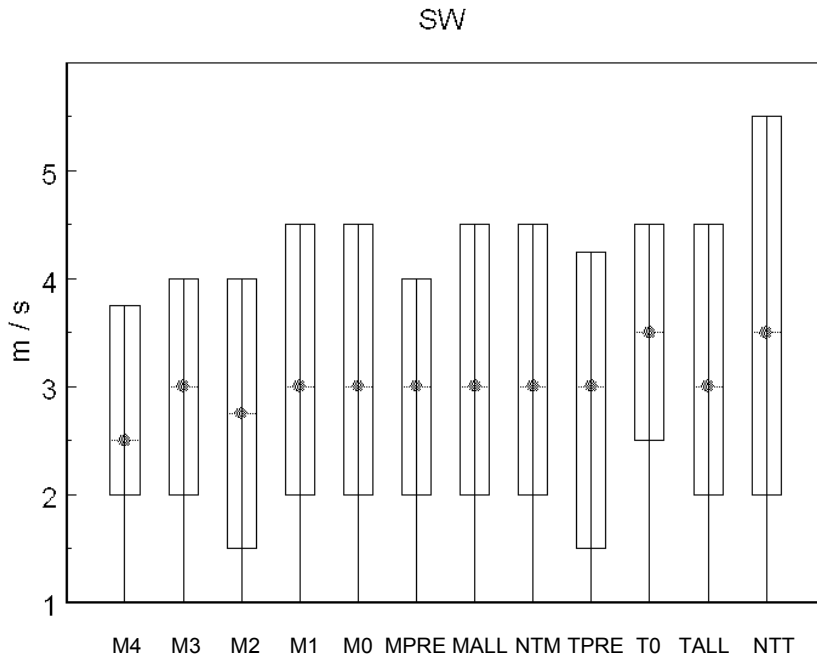


Fig. 24. As in Fig. 6, except for SW.

We next consider larger arrays of SW in the hope of extracting a signal from the inherent background noise in the raw data (Fig. 2). We hypothesize that differences will be more apparent than observed in Fig. 24 when only the centroid bin was considered. We also hypothesize that greater values of LLDV will be associated with greater values of SW.

The first hypothesis can be tested by comparing Fig. 24 and Fig. 25 containing the SW and SW5 arrays. Somewhat greater differences among the datasets are evident in the larger array. Specifically, there are larger values for T0 detections as well as a steadier increase from

M4 through M0. When Fig. 25 is compared to Fig. 6 (LLDV) we see a similar steady increase between M4 through M0 and the pronounced difference between TPRE and T0. These aspects were much less evident between Fig. 24 and Fig. 6. Box plots of SW7, SW9, and SW11 (not shown) yield results similar to Fig. 25. These findings suggest that a stronger signal is extracted from a larger array than a single element; however, the incremental improvements gradually decrease with increasing array size. Overall, the differences between Fig. 24 and Fig. 25 suggest that averaging SW over an array can mitigate noise in the data while preserving useful information.

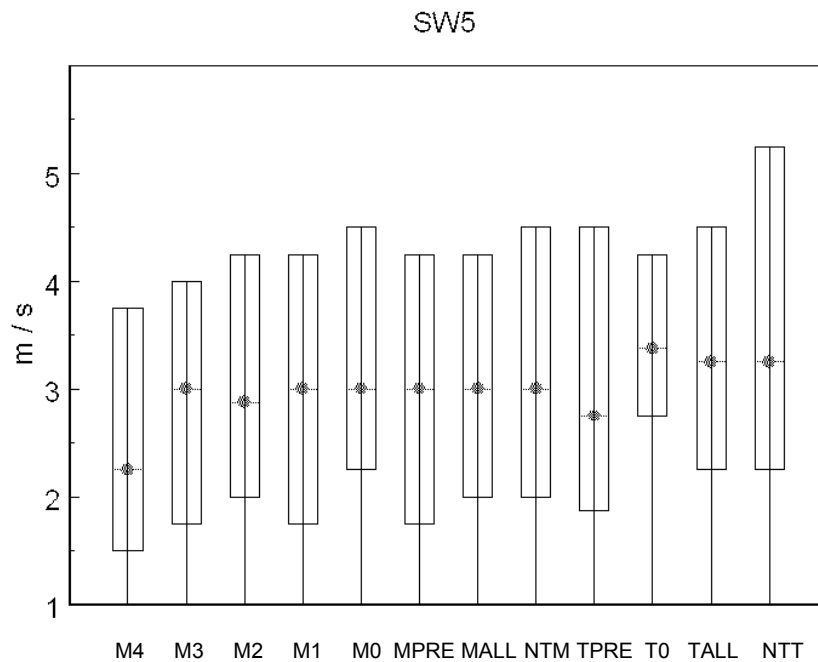


Fig. 25. As in Fig. 6, except for SW5.

According to the second hypothesis, SW should be greatest for T0 detections, followed by TPRE and NTT (Fig. 6). However, what actually is observed (Fig. 24 and Fig. 25) is a significant increase from TPRE to T0, which is expected, and little difference between T0 and NTT. This unexpected finding suggests that pre-tornadic circulations may possess more laminar flow than both tornadic and non-tornadic detections, yielding smaller values of spectrum width.

We hypothesized that tornadic and pre-tornadic circulations would be stronger, more turbulent, and therefore associated with larger SW than non-tornadic storms. However, the data suggest generally smaller values for the tornadic circulations, especially with the pre-tornadic dataset. This trend is observed in both mesocyclone and TVS detections. Furthermore, at the time of tornado occurrence (M0 and T0), the difference in median values from the non-tornadic datasets is smallest. This suggests that the MPRE and TPRE circulations might exhibit less

turbulent helical flow prior to stretching and shrinking into a tornadic state when the turbulence increases to make the differences negligible between the NTM and NTT detections.

The correlation matrix of MALL for different SW array sizes reveals a trend toward greater correlations as the arrays become larger (Fig. 26). This trend is quantified by the correlation coefficients in Table 14. For example, the correlations between SW and SW5, and SW5 and SW7 are 0.898 and 0.967, respectively. For SW9 and SW11, the correlation increases to 0.988. For the NTM detections, the trend is similar; however, the correlation coefficients generally are larger (Table 15). The greater correlations among the NTM arrays suggest greater continuity in the local SW fields compared to the SW fields associated with MALL detections. Fig. 26 and Table 15 also indicate that important information is obtained when using a small data array instead of a single bin; however, the amount of unique information decreases as the array size becomes even larger. Based on this finding, and the earlier discussion comparing Fig. 24, Fig. 25, and Fig. 6, we conclude that relatively small SW arrays are better able to discriminate between tornadic and non-tornadic detections than single bins. However, the difference is small. Among the tornadic detections, the similar correlation coefficients in Table 16 and Table 17 suggest that this assumption is equally valid for both subsets of MALL.

I next performed a two-sample Kolmogorov-Smirnov goodness of fit test between pairs of detections for several array sizes (Table 13) to determine whether there is a statistically significant difference between the tornadic and non-tornadic SW detections. Based on a threshold p-value of 0.05, the results show statistically significant differences between the NTM and MALL datasets, especially for the larger array sizes. Statistically significant differences also are observed between the NTM and MPRE datasets, although there appears to be no relation between array size and either p- or t-values. Conversely, there are no statistically significant differences between the NTM and M0 or the NTT and T0 datasets for any array size. This was observed qualitatively in Fig. 25. Overall, the differences between the tornadic and non-tornadic TVS detections are less significant than between the tornadic and non-tornadic mesocyclone detections. This may be due partly to the much smaller dataset of TVS detections (Table 4).

The qualitative assessment of SW favors the use of larger arrays to discriminate between tornadic and non-tornadic detections. And, statistical analyses indicate that the largest arrays perform the best, even though the qualitative differences between the medium sized arrays and the largest arrays are minor. These results suggest that I concentrate on the largest arrays. Nonetheless, since these parameters have not been examined thoroughly in previous studies, I will keep all array sizes in subsequent analyses to further test their usefulness.

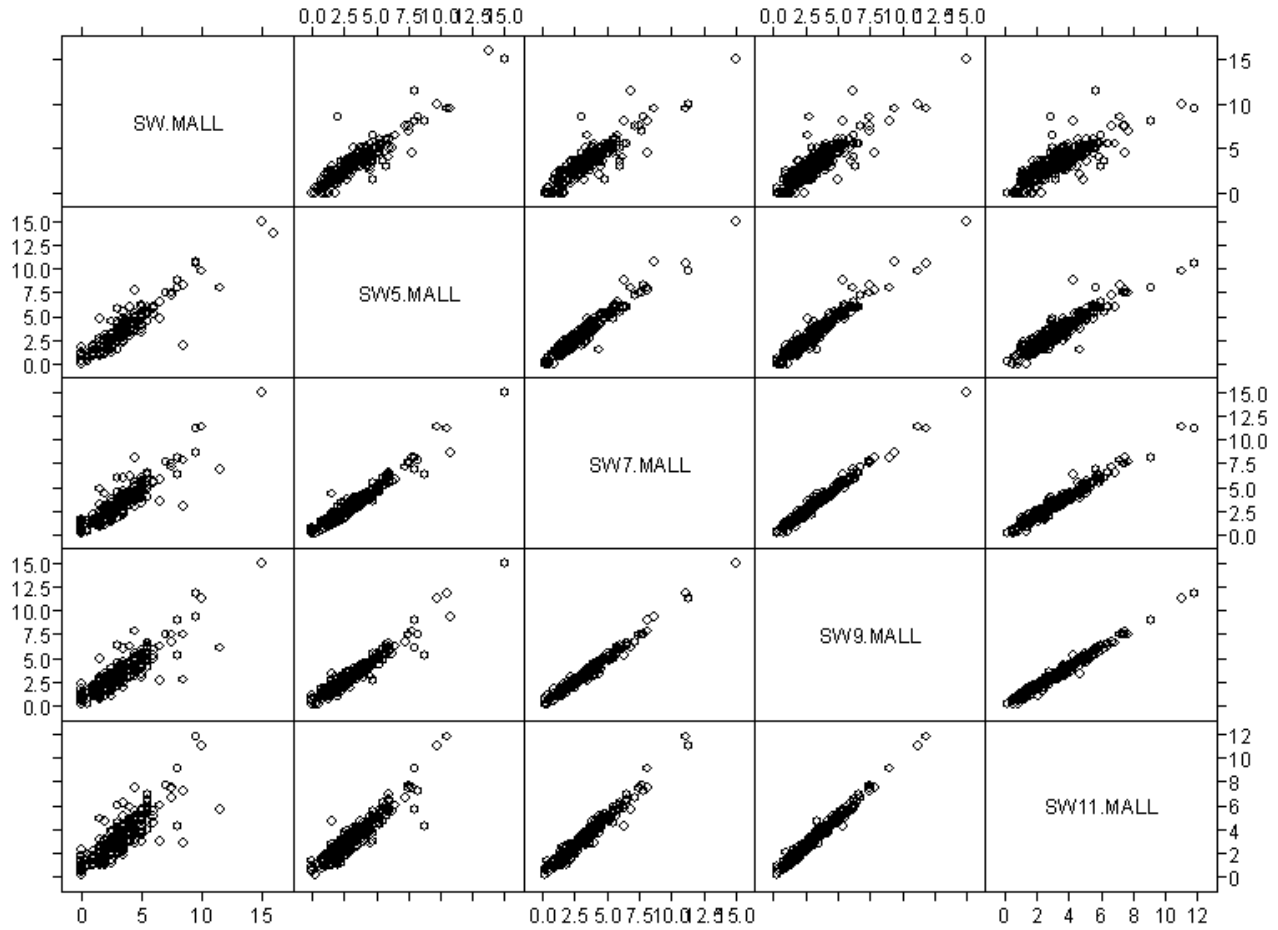


Fig. 26. Scatter plot correlation matrix for all arrays of MALL SW.

Table 14. Correlation coefficients the different arrays of MALL SW.

SW.MALL	0.898	0.876	0.847	0.834
	SW5.MALL	0.967	0.955	0.933
		SW7.MALL	0.987	0.978
			SW9.MALL	0.988
				SW11.MALL

Table 15. As in Table 14, except for NTM detections.

SW.NTM	0.964	0.957	0.948	0.943
	SW5.NTM	0.986	0.982	0.974
		SW7.NTM	0.992	0.989
			SW9.NTM	0.995
				SW11.NTM

Table 16. As in Table 14, except for MPRE detections.

SW.MPRE	0.917	0.882	0.857	0.831
	SW5.MPRE	0.962	0.949	0.915
		SW7.MPRE	0.986	0.971
			SW9.MPRE	0.985
				SW11.MPRE

Table 17. As in Table 14, except for M0 detections

SW.M0	0.875	0.868	0.836	0.837
	SW5.M0	0.974	0.964	0.955
		SW7.M0	0.989	0.986
			SW9.M0	0.991
				SW11.M0

Table 18. Regression tree inclusion matrix for SW arrays. Arrays appearing in regression trees are denoted with a “Yes”. The numbers below each Yes designation indicate the split in which the SW array appeared. The following number indicates the threshold at which the split occurred in $m s^{-1}$.

	n = 1	n = 5	n = 7	n = 9	n = 11
SWn.NTM / SWn.MALL	No	No	No	No	No
SWn.NTM / SWn.MPRE	No	No	No	No	No
SWn.NTM / SWn.M0	No	No	No	No	No
SWn.NTT / SWn.TALL	No	No	No	Yes 3 < 1.7	Yes 3 < 1.6
SWn.NTT / SWn.TPRE	No	No	No	No	No
SWn.NTT / SWn.T0	No	No	Yes 3 < 2.3	Yes 3 < 2.3	Yes 3 < 2.0

I next compared all SW arrays in a variety of regression trees to test their predictive abilities when used together with the SSAP diagnostic parameters discussed earlier. TSI and SW9 thresholds remain as a combination showing more impressive predictive power.

Table 18 summarizes the basic characteristics of each tree. A “No” designation means

that the particular SW array was not selected in the tree for that particular comparison. For the mesocyclone detections, the same predictors (VIROTV and LLDV) are dominant over every SW array size. For the TVS comparisons, only the larger SW arrays appear in some trees (Table 18). This suggests that the larger SW arrays have predictive ability that is comparable to the four TDA predictors used in the regression trees (Table 6). A particularly encouraging example is shown in Fig. 27, where SW9 is used for the NTT versus T0 detections. If $TSI \geq 1571$ and $LLDV < 57.0$, then having $SW9 \geq 2.3 \text{ m s}^{-1}$ yields a 20.8% success rate for discriminating between these detections. Since the LLDV condition is nearly always met, the TSI and SW9 thresholds remain as a combination showing impressive predictive power.

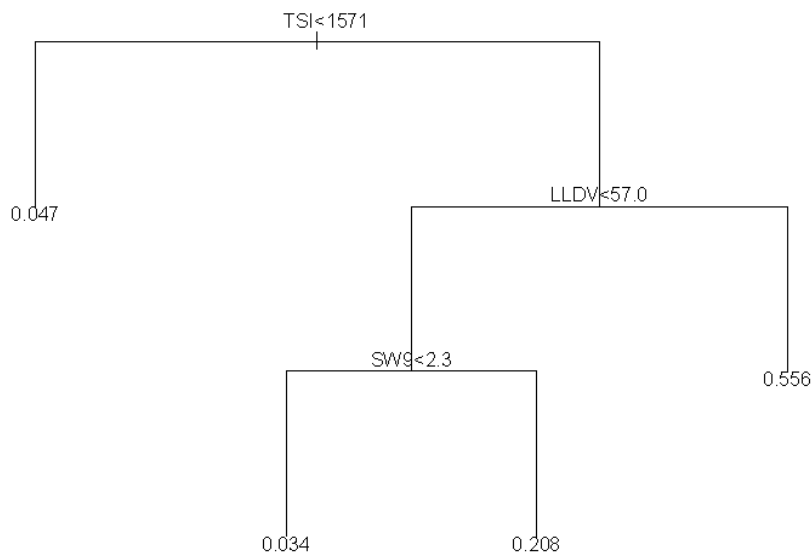


Fig. 27. Regression tree for NTT versus T0 detections using the TVS parameters in Table 6 with SW9.

To summarize, qualitative differences appear between certain tornadic and non-tornadic datasets of SW, especially as their array size is increased. Unfortunately, based on the box and whisker diagrams, these differences usually will be too small to make SW an effective sole discriminator in an operational environment where analysis tends to be qualitative. The larger SW arrays show statistically significant skill in discriminating between tornadic and non-tornadic detections. Finally, regression trees containing both the SSAP predictors and various SW arrays reveal many cases when SW is at least comparable to the best TDA parameters at discriminating between tornadic and non-tornadic detections.

3.2.2 Azimuthal Shear

Azimuthal Shear (AZ) is defined by Smith et al. (2003) as the rotational component of the 2-dimensional local linear least squares (LLSD) of Velocity (V). It is described by the following equation:

$$u_s = \frac{\sum S_{ij} V_{ij} w_{ij}}{\sum (\Delta S_{ij})^2 w_{ij}}, \quad (4)$$

where V_{ij} is the radial velocity, s_{ij} is the azimuthal distance from the center of the kernel to the point (i,j) , and w_{ij} is a uniform weight function. As noted in Smith et al., AZ approximates one half the vertical vorticity, assuming a symmetric wind field. Velocity data are passed through a 3 X 3 median filter to reduce noise. Missing values of V are filled in with the median of the four adjacent bin values of V.

AZ is the second new parameter that we consider. As discussed in Section 3.2 and Table 12, the smallest array sizes were preferred because of the filtering that is already applied to reduce noise. Based on subjective analyses of the AZ7, AZ9, and AZ11 arrays (not shown), the AZ, AZ5, and AZ7 arrays were selected for further study. AZ3 was omitted because this array size yielded the same results as AZ. Because mesocyclones and TVSSs are almost exclusively cyclonic, I hypothesized that values of AZ mostly should be positive, i.e., with cyclonic shear. As with SW, AZ only is considered at the lowest radar elevation slice.

We begin by qualitatively assessing the normality of AZ using probability distribution histograms (Fig. 28 and Fig. 29). These distributions are much more symmetrical and normal than the SW distributions (Fig. 20-Fig. 23), probably because AZ can be both negative and positive, whereas SW always is positive.

The hypothesis that AZ mostly should be positive is refuted by Fig. 28 and Fig. 29, which show not only symmetry near zero in all cases, but also a slightly negative mode for the MALL and TALL distributions. This contrasts with the NTM and NTT distributions which show a slightly positive mode. This finding indicates that anticyclonic shear frequently is observed, especially with the MALL and TALL datasets. As illustrated with the separate 2-dimensional segments in Fig. 1, it would be possible to have anticyclonic shear in the lowest elevation slice that is coincident with the centroid of a mesocyclone or TVSS detection. In the case of the mesocyclone, it would not be necessary to have a cyclonic shear region in the lowest elevation slice. Still, it is

surprising to see slightly negative modality in the lowest elevation slice for the M0 and T0 detections (Fig. 30) since the non-descending mode of tornadogenesis predicts a preponderance of cyclonic shear in the lowest levels of the storm during the tornado.

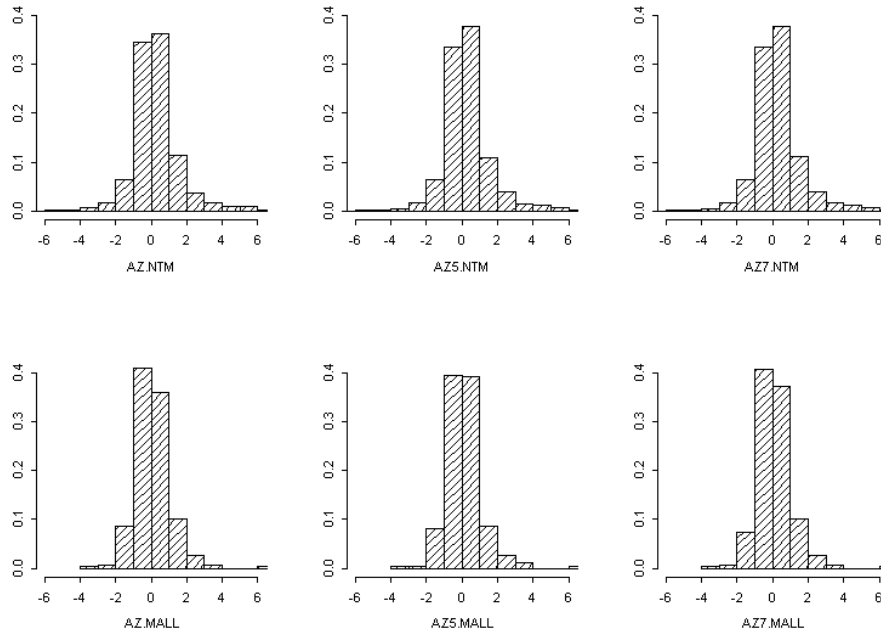


Fig. 28. As in Fig. 20 and Fig. 21, except for Azimuthal Shear with Non-Tornadic Mesocyclones (NTM) and all Tornadic/Pre-tornadic Mesocyclones (MALL).

Kolmogorov-Smirnov two sample goodness-of-fit tests on AZ datasets indicate that there is a statistically significant difference between the Non-Tornadic Mesocyclones (NTM) and both the tornadic/pre-tornadic mesocyclones (MALL) and the mesocyclones associated with tornado occurrence (M0; Table 19). To a lesser extent, a statistically significant difference also exists between the Non-Tornadic TVVs (NTT) and the tornadic/pre-tornadic TVVs (TPRE).

Fig. 31 is a box and whisker plot for AZ. The slight positive skewing seen in the NTM and NTT distributions (Fig. 29) is confirmed, as is the negative skewing for TPRES, T0, and TALL. There is surprising symmetry about zero for the mesocyclone detections associated with a tornado. The M3 detections stand out as being strongly positive compared to the other pre-tornadic categories. In fact, the M3 category likely is the reason why the MPRES dataset has slightly positive skewness. This is reminiscent of the anomalously large M3 values seen with Low-Level Convergence (LLCONV; Fig. 9). Although this raises the question of whether the two parameters are related, they exhibit a very small correlation coefficient (-0.036). Such a small correlation is not surprising since AZ considers the rotational component of the local linear least-squares derivative, whereas LLCONV is associated with the divergent component of adjacent

bins of V at the same azimuth (Fig. 19).

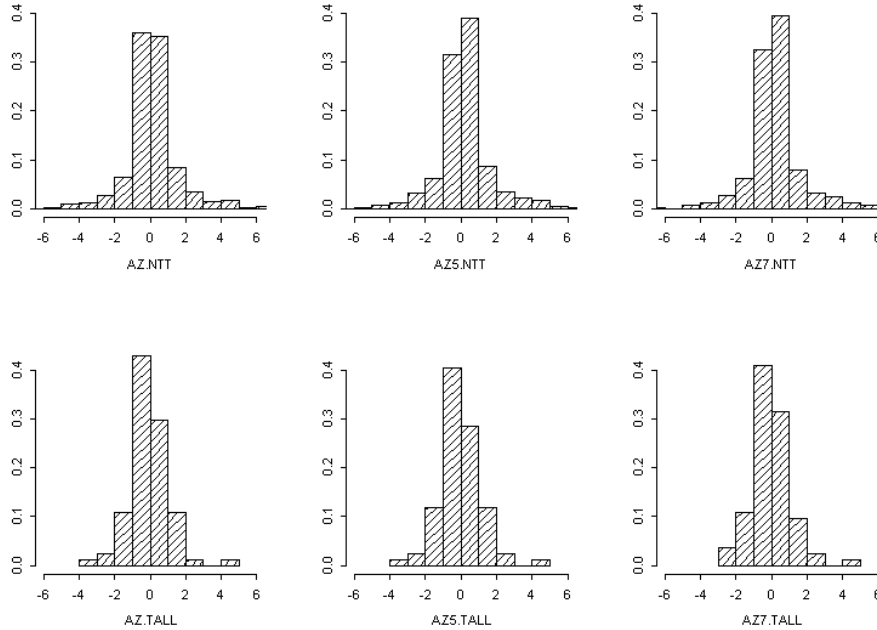


Fig. 29. As in Fig. 22 and Fig. 23, except for Azimuthal Shear with Non-Tornadic TVS detections (NTT; top) and all Tornadic/pre-tornadic TVS detections (TALL; bottom). Array sizes from left to right are 1,5, and 7.

The AZ5 array exhibits a similar distribution (Fig. 32). There is slightly more positive skewing for the tornadic and pre-tornadic mesocyclone detections, but results for the other detections strongly resemble those of AZ (Fig. 31). The AZ7 array (Fig. 33) possesses similar characteristics. The most variation occurs in those quantities having the fewest members (i.e., M4 and M3; Table 4). Still, it is unclear why M3 is so strongly positive.

Correlation coefficients were computed between each array size for each of the datasets listed in the abscissas of Fig. 31 - Fig. 33. Most comparisons exhibit a correlation coefficient > 0.95 , and every comparison exhibits a correlation > 0.9 (not shown). We conclude that AZ changes little with array size. This finding also is supported by the qualitative comparison of Fig. 31-Fig. 33. The result is not surprising since AZ smooths the V data *a priori*. Therefore, larger arrays should provide negligible additional smoothing.

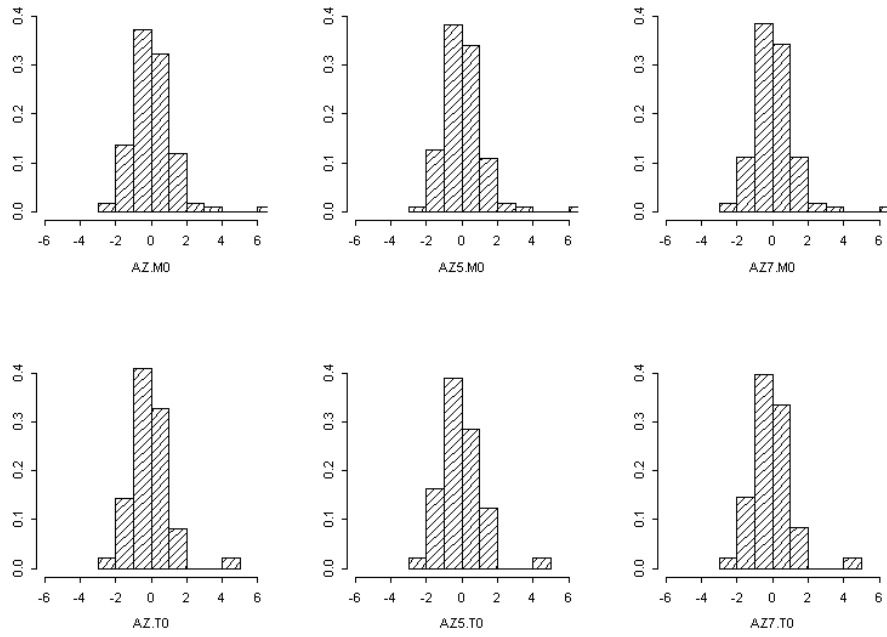


Fig. 30. As in Fig. 20, except for AZ arrays with M0 and T0 datasets.

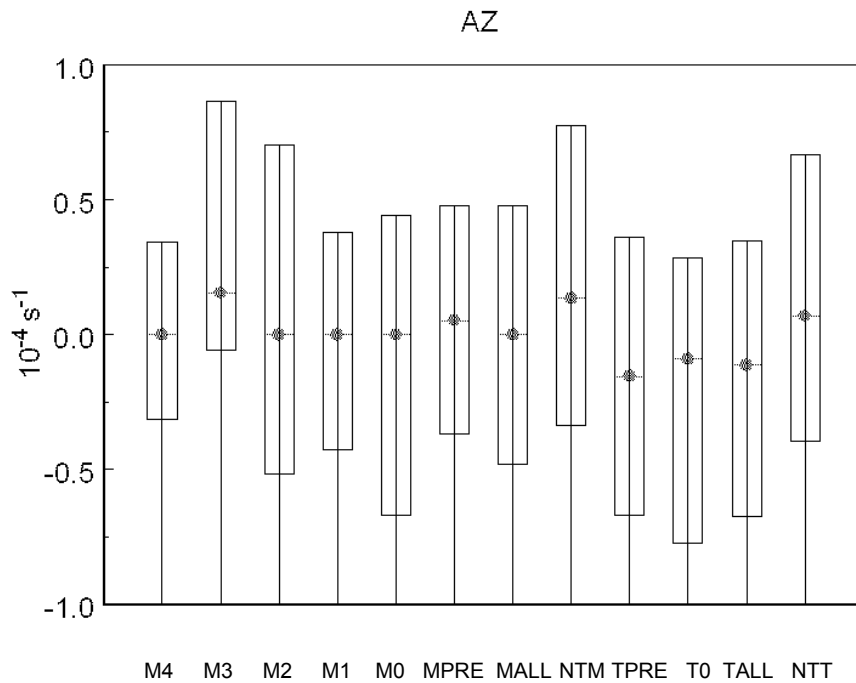


Fig. 31. As in Fig. 6, except for AZ.

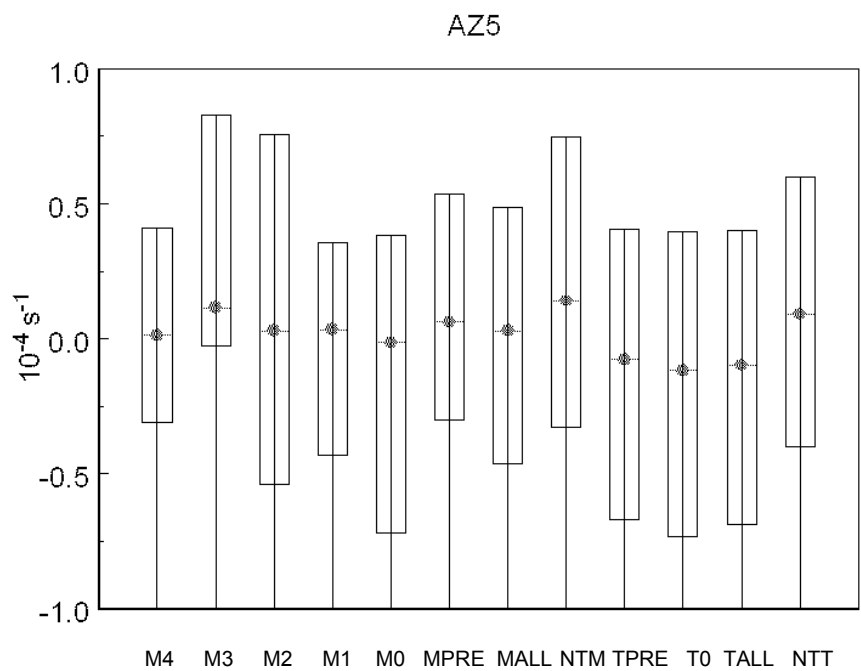


Fig. 32. As in Fig. 31, except for AZ5

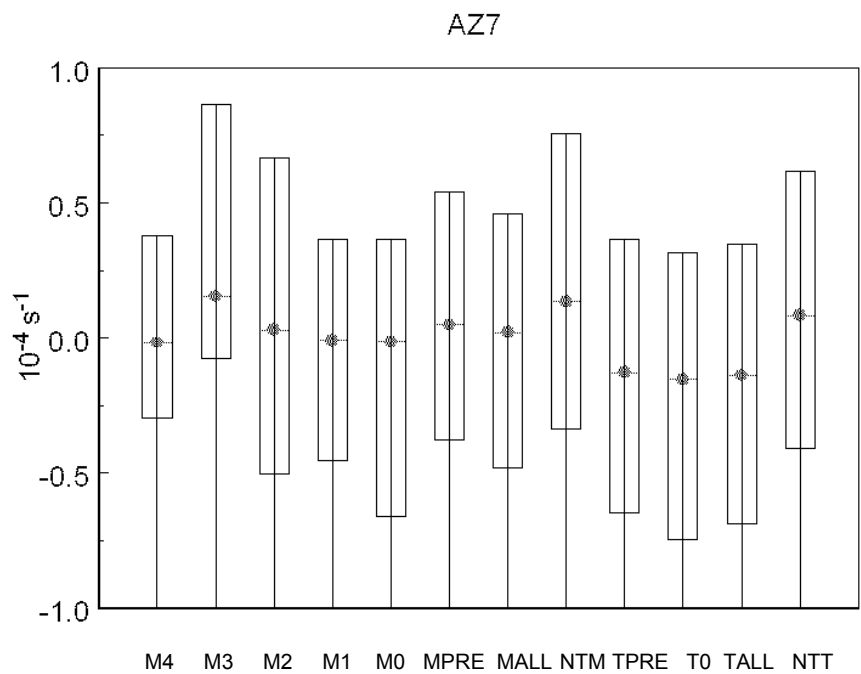


Fig. 33. As in Fig. 31, except for AZ7.

Table 19. As in Table 13, except for different array sizes of Azimuthal Shear (AZ).

	n = 1	n = 5	n = 7
AZn.NTM / AZn.MALL	0.12 0.00	0.12 0.00	0.11 0.00
AZn.NTM / AZn.MPRE	0.10 0.09	0.09 0.20	0.09 0.19
AZn.NTM / AZn.M0	0.15 0.01	0.18 0.00	0.15 0.01
AZn.NTT / AZn.TALL	0.19 0.01	0.16 0.06	0.19 0.01
AZn.NTT / AZn.TPRE	0.21 0.10	0.19 0.15	0.19 0.18
AZn.NTT / AZn.T0	0.18 0.08	0.17 0.13	0.20 0.05

Table 20. As in Table 18, except for AZ in units of ($10^{-4} \times s^{-1}$).

	n = 1	n = 5	n = 7
AZn.NTM / AZn.MALL	No	No	No
AZn.NTM / AZn.MPRE	Yes 3 < 1.05	Yes 3 <0.99	Yes 3 < 1.03
AZn.NTM / AZn.M0	No	No	No
AZn.NTT / AZn.TALL	Yes 3 < 2.14	Yes 3 < -0.58	Yes 3 <2.12
AZn.NTT / AZn.TPRE	No	No	No
AZn.NTT / AZn.T0	No	No	No

Two-sample Kolmogorov-Smirnov goodness of fit tests show that the most statistically significant differences occur between the non-tornadic and tornadic/pre-tornadic AZ datasets (NTM versus MALL; Table 19), and also between the NTM and tornadic (M0) datasets. Every other comparison does not meet the 0.05 confidence threshold. A few cases in the non-tornadic TVS (NTT) versus tornadic/pre-tornadic TVS (TALL) comparison also exhibit statistically

significant differences. Overall, more statistically significant differences are observed compared to SW (Table 13). Therefore, we conclude that AZ exhibits better ability than SW at discriminating between tornadic and non-tornadic mesocyclones.

Regression trees were created using the SSAP parameters (Table 11) and each of the AZ array sizes to determine if AZ has comparable predictive skill. The results are summarized in Table 20. Each AZ array size appears in the third split of the NTM / MPRE comparisons (Table 20) following two splits of VIROTV (not shown). Comparison with the SSAP-only results (Fig. 15) shows that AZ arrays appear to have predictive skill comparable to LLDV. An example is shown in Fig. 34. One terminal node below the AZ5 split produces a successful detection rate of 8.6%. This is comparable to the success rate of 8.4% in the right terminal node below LLDV in Fig. 15.

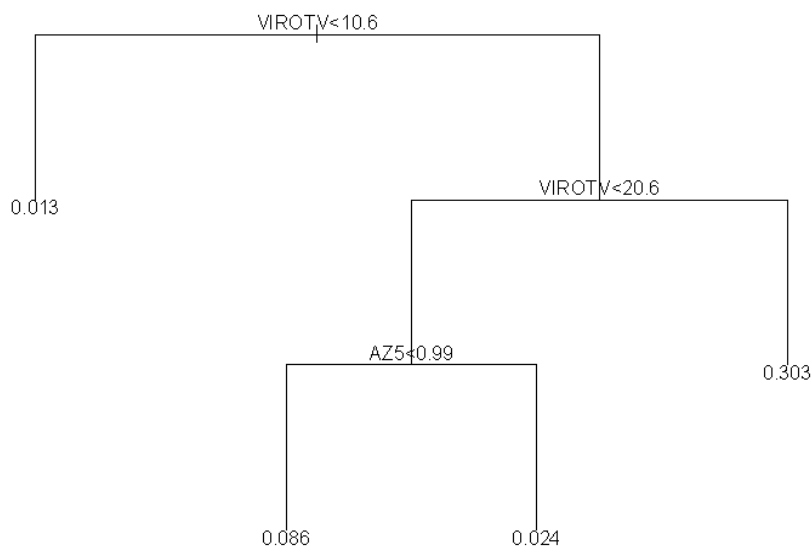


Fig. 34. As in Fig. 14, except including AZ5 in units of 10^{-4} s^{-1} .

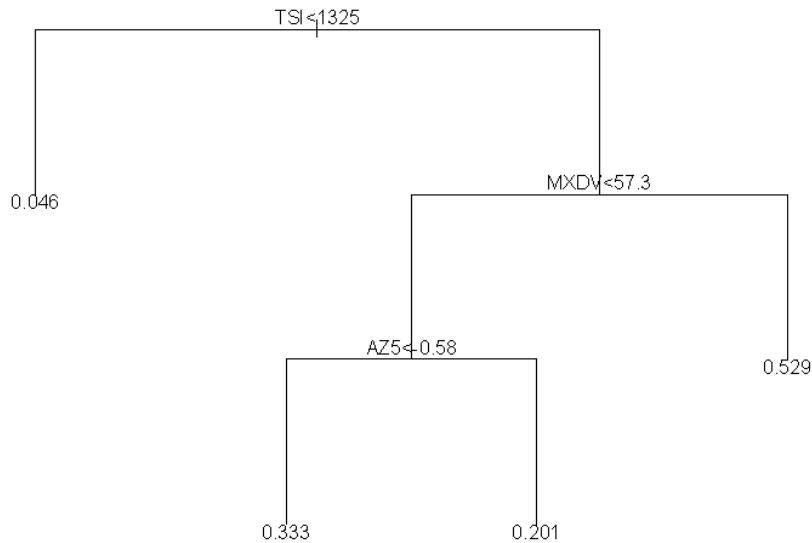


Fig. 35. NTT versus TALL comparison with TDA parameters (Table 11) and including AZ5 in of units of 10^{-4} s^{-1} .

Similar to the MDA results, each AZ array appears in the third split of the NTT versus TALL comparison (Table 20). A particularly interesting example is shown in Fig. 35. AZ5 appears immediately after MXDV, which Marzban (2001) showed to be a dominant discriminator of tornadic TVSs. This is the only case in which the AZ threshold is less than zero ($-0.58 \times 10^{-4} \text{ s}^{-1}$). There is a greater probability of a successful detection (33.3%) if AZ5 is less than this value. As noted earlier, this is a surprising result since we assumed that AZ would be strongly positive to reflect the strong cyclonic shear associated with the imminent or occurring tornado.

Regression trees were constructed using combinations of SSAP, AZ and SW parameters. Both AZ and SW had to appear in the original comparisons to be considered (Table 18 and Table 20). Specifically, only the larger array sizes for the NTT versus TALL comparison were considered because these were the only occurrences exhibiting overlap between the two predictors. The SW array appears instead of the AZ array (not shown) in all of the new regression trees. This indicates that SW is a more robust predictor than AZ when used in combination with the SSAP parameters.

To summarize, AZ statistically exhibits less utility than SW at differentiating between tornadic and non-tornadic detections when used alone. However, when used in regression trees

together with SSAP parameters, AZ exhibits utility comparable to SW for TVS detections and is superior to SW for mesocyclone detections. When SW and AZ arrays are combined to create regression trees, SW always emerges as the dominant predictor. A surprising finding is the preponderance of negative AZ values in the T0, TALL, and TPRE detections. Conversely, the NTT detections are predominantly positive. There currently is no good explanation for why the tornadic TVS detections have a strong negative mode. This is a subject for future study.

3.2.3 Reflectivity Variance

The local variance of Reflectivity (REV) is the final new parameter that we examine for forecasting utility. The Introduction described numerous observational studies and simulations (e.g., Wakimoto et al. 1998, Lemon 1980, Weisman and Klemp 1982) showing that tornadoes typically are associated with strong horizontal RE gradients. An enhanced horizontal gradient would produce a large REV. I hypothesized that tornadic detections would have larger REV values than non-tornadic detections. I also expected gradually increasing REV prior to tornado occurrence and maximum REV during the tornado. However, it should be noted that large REV can result from noisy data, as illustrated in Fig. 36. This possible misrepresentation must be considered as we investigate REV.

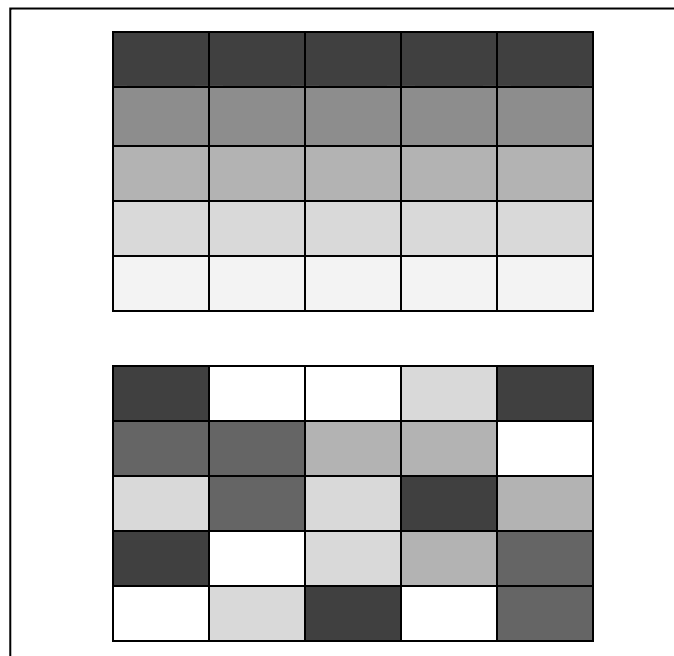


Fig. 36. Schematic of two 5 X 5 arrays of Reflectivity. Darker blocks represent radar bins with relatively large values of Reflectivity. Both arrays have equal variances, but unequal gradients of Reflectivity.

We begin by examining histograms of REV (Fig. 37-Fig. 39). Each diagram reveals significant positive skewing, likely because variance is the square of standard deviation, and

therefore always is positive. Skewness for each dataset decreases as array size increases. This likely is due to the larger arrays providing larger populations with more positive outliers that exert a disproportionate influence on the right tail of the distribution.

We next investigate box and whisker plots of REV for different array sizes. For RE5V (Fig. 40), the median variance gradually decreases in the M4 through M0 detections, with a more pronounced decrease in the 75th percentile variance value (i.e., the upper border of each box). The exception is the M1 dataset whose values are comparable to the M4 category. Overall, the MPRE detections show greater variance than the NTM detections. The opposite is true for TPRE versus NTT detections.

These results for mesocyclones are contrary to what we expected—the tornadic cases do not exhibit the greatest REV. One possible reason is that mesocyclone occlusion during tornadogenesis may reduce the reflectivity gradient that has been observed prior to the tornado. However, this does not explain why the same trend is not observed with the TVS detections.

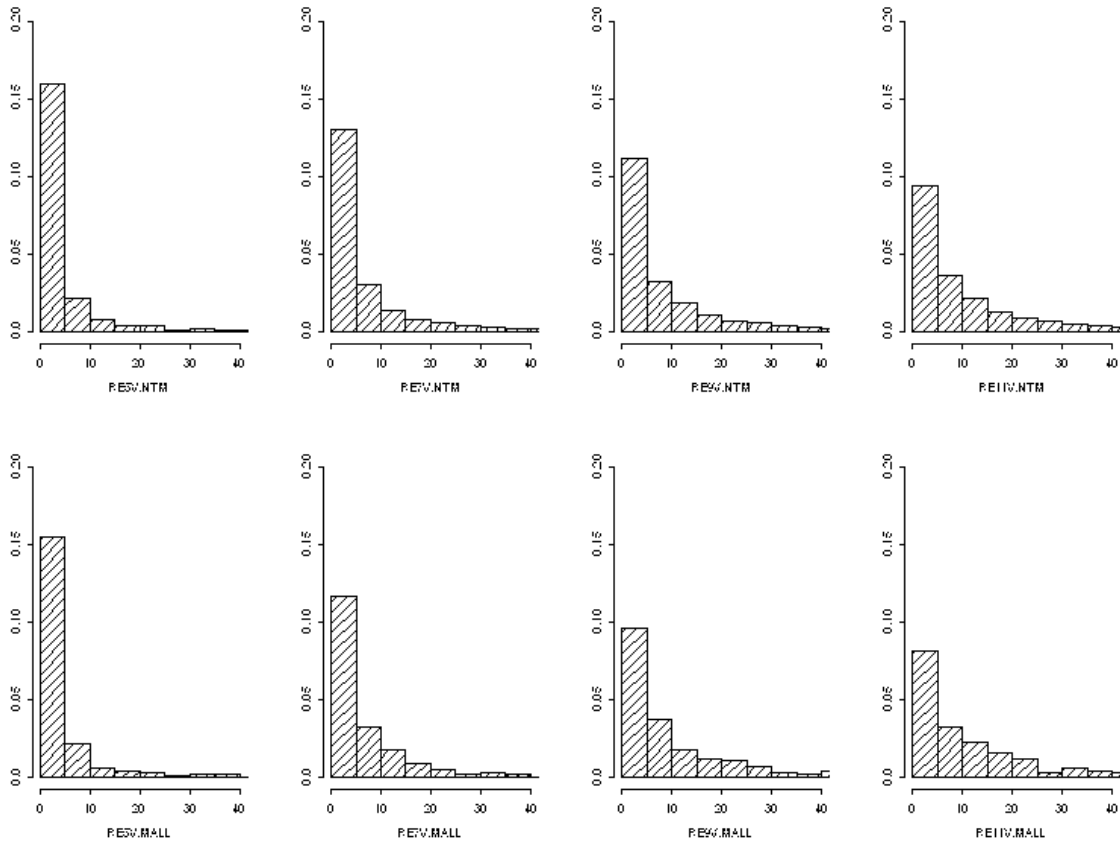


Fig. 37. As in Fig. 20, except for REV. The arrays are labeled RE#V, where # is the array size (see Fig. 36 for an illustration of array sizes). The top row is non-tornadic mesocyclones (NTM), the bottom row is tornadic/pre-tornadic mesocyclones (MPRE), and array sizes from left to right are 5,7,9, and 11.

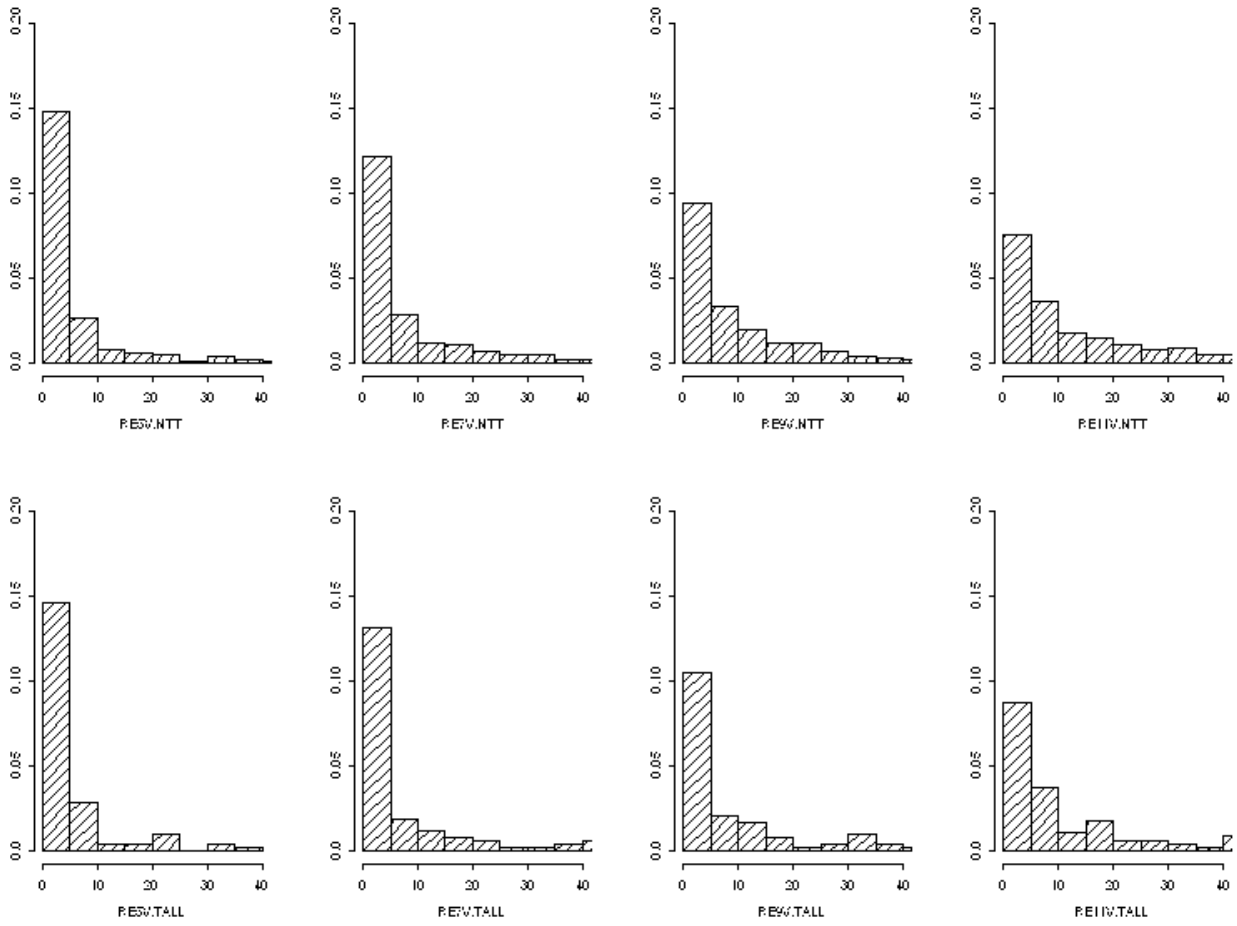


Fig. 38. As in Fig. 37, except for NTT (top) and TALL (bottom).

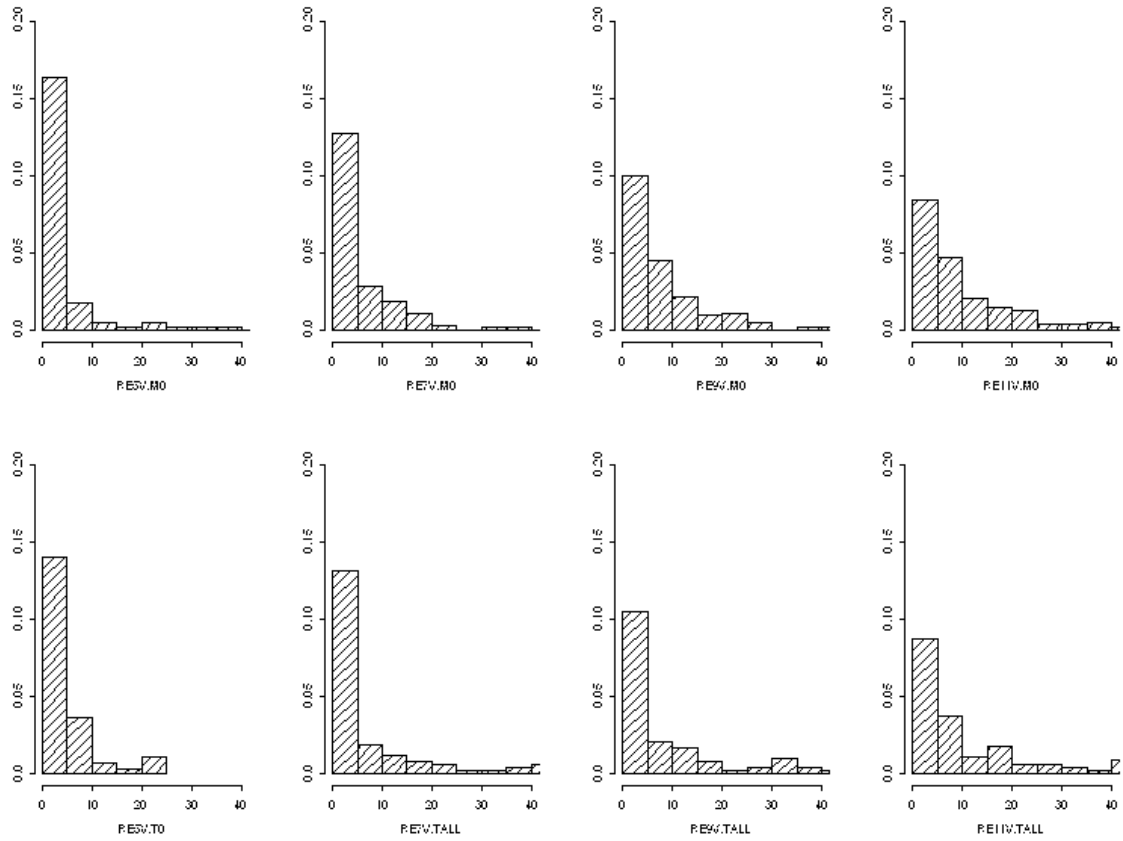


Fig. 39. As in Fig. 37, except for M0 (top) and T0 (bottom).

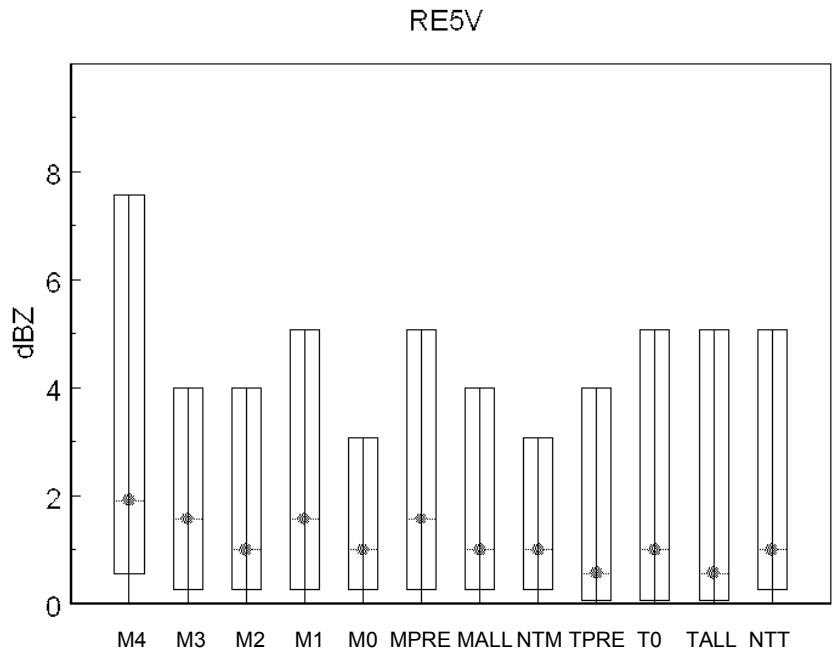


Fig. 40. As in Fig. 6, except for RE5V.

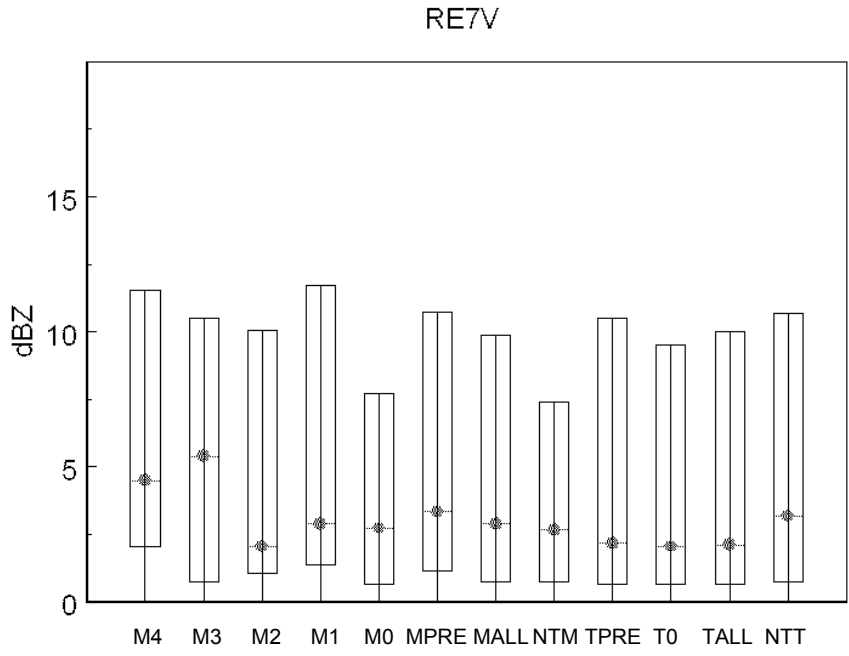


Fig. 41. As in Fig. 6, except for RE7V.

The RE7V arrays produce similar results (Fig. 41). The greater range of ordinate values indicates that the variance is greater than in the RE5V arrays. Since we assume that mesocyclone and TVS detections are associated with a reflectivity gradient (e.g., see Lemon 1980), larger arrays should sample data across a larger part of the gradient and thereby produce

greater variance. Even with this sampling difference, both Fig. 40 and Fig. 41 show similar qualitative differences among their respective datasets. The exception is the M3 dataset which exhibits a large increase in median values in the RE7V array (Fig. 41). It is unclear why this occurs.

REV trends for the M4 through M0 datasets are relatively smooth in the RE9V arrays and smoothest in the RE11V arrays (Fig. 42 and Fig. 43, respectively). The overall increase in variance seen in Fig. 40 - Fig. 42 appears to end at the largest array size, i.e., RE11V (Fig. 43). Therefore, we expect arrays larger than RE11V to exhibit little additional differences among the datasets (not shown). The RE11V array exhibits better consistency between mesocyclone and TVS detections than the RE5V array. Specifically, median variances for both MPRE and TPRE are greater than those for M0 and T0, respectively. However, there still is inconsistency between the M0 versus NTM and T0 versus NTT differences, since the former pair is approximately equivalent while the latter pair shows NTT with clearly larger overall values.

Based on the trends described above, I conclude that the largest array size best ensures a robust calculation of variance. And, contrary to what I hypothesized, pre-tornadic mesocyclone and TVS detections exhibit larger variances than do tornadic detections. This unexpected finding requires further investigation.

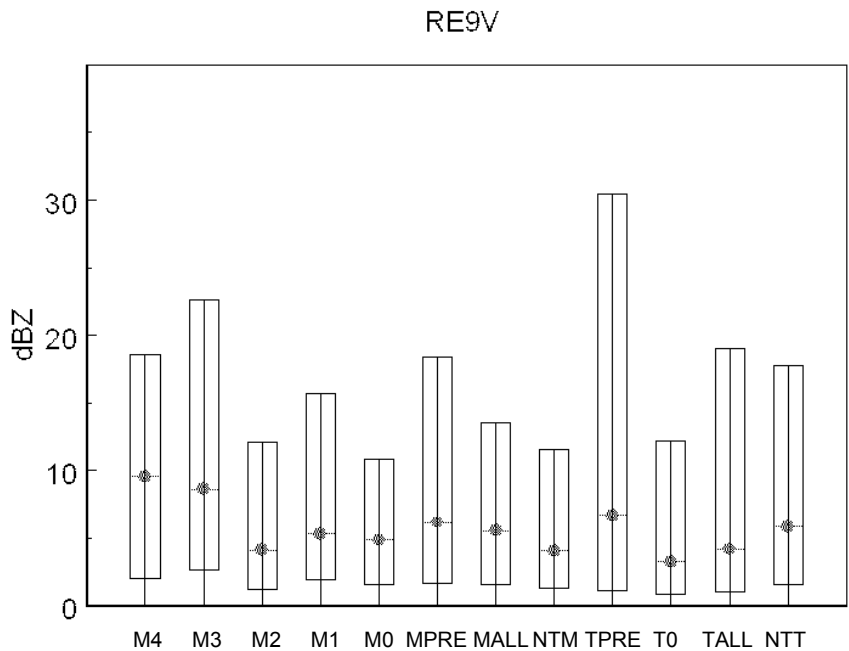


Fig. 42. As in Fig. 6, except for RE9V.

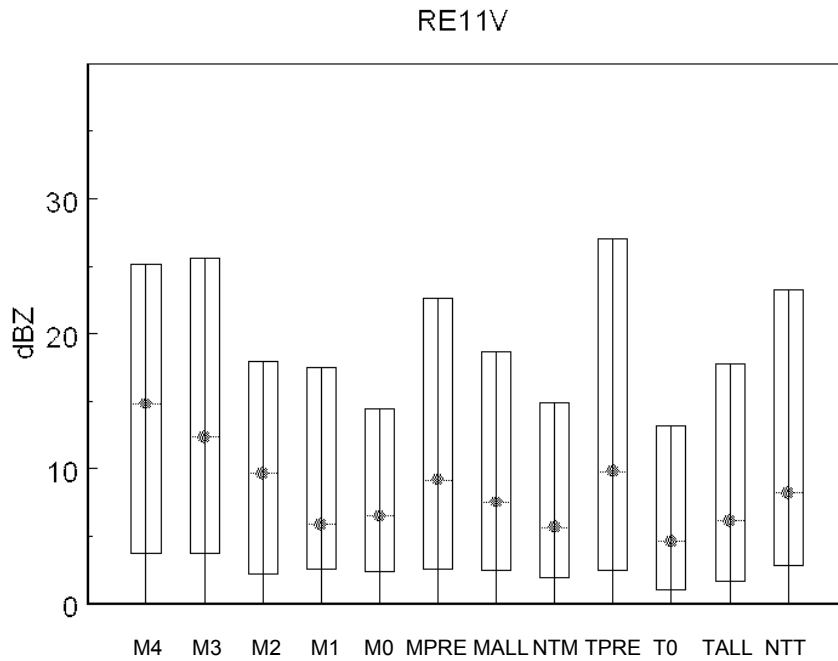


Fig. 43. As in Fig. 6, except for RE11V.

Table 21. Correlation coefficients for the REV arrays. Coefficients above the gray diagonal are for the tornadic and pre-tornadic mesocyclone detection (MALL) datasets. Coefficients below the diagonal are for the NTM datasets.

RE5V	0.672	0.677	0.597
0.703	RE7V	0.788	0.731
0.670	0.806	RE9V	0.869
0.538	0.786	0.872	RE11V

Table 22. Correlation coefficients for the REV arrays. Coefficients above the gray diagonal are for the MPRE datasets. Coefficients below the diagonal are for the M0 datasets.

RE5V	0.749	0.719	0.623
0.536	RE7V	0.763	0.725
0.523	0.862	RE9V	0.883
0.506	0.745	0.830	RE11V

The pronounced differences among the different array sizes (Fig. 40 - Fig. 43) are confirmed by smaller correlation coefficients among the MALL, NTM, MPRE, and M0 datasets (Table 21 and Table 22) compared to the SW arrays (Table 14-Table 17) and AZ arrays (not shown). This indicates a greater likelihood of extracting different results with increasing array size. Results from the larger arrays appear to be most useful (Fig. 43); however, the REV array

sizes appear to have an upper limit of usefulness near size 11.

Despite the large qualitative differences among the datasets for each array size, Kolmogorov-Smirnov goodness-of-fit tests show that statistically significant differences exist only for the NTM versus MPRE and for the larger array sizes of NTM versus MALL comparisons (Table 23). We therefore conclude that REV by itself does not exhibit skill at discriminating between tornadic and non-tornadic detections, although there may be some skill for non-tornadic versus pre-tornadic detections.

Regression trees were created using the SSAP parameters (Table 11) and each of the REV arrays to determine if the addition of REV enhances predictive skill. Results for mesocyclones (Table 24) indicate that REV does not show skill comparable to the best SSAP diagnostics. However, for TVS detections, larger REV arrays appear in regression trees for the NTT versus TALL comparisons, while smaller arrays appear in regression trees for the NTT versus TPRES comparisons. When REV appears in a decision tree, it nearly always is located at the second split instead of the third split, as observed with SW (Table 18). This suggests that REV has better predictive ability than SW for the TVS datasets. An example is shown in Fig. 44 for the NTT versus TALL comparison using RE11V. A combination of $TSI \geq 1367$ and $RE11V < 0.62$ yields an impressive 46.4% success rate. This supports the requirement for small REV to accompany T0 or M0 detections. We conclude that small values of REV in the larger arrays have utility in identifying tornadic TVSs when used with other SSAP predictors.

Table 23. As in Table 13, except for REnV arrays.

	n = 5	n = 7	n = 9	n = 11
REnV.NTM / REnV.MALL	0.07	0.08	0.09	0.08
	0.09	0.06	0.02	0.05
REnV.NTM / REnV.MPRE	0.10	0.11	0.12	0.14
	0.05	0.04	0.02	0.00
REnV.NTM / REnV.M0	0.04	0.05	0.06	0.06
	0.98	0.88	0.72	0.71
REnV.NTT / REnV.TALL	0.10	0.12	0.09	0.11
	0.31	0.20	0.56	0.28
REnV.NTT / REnV.TPRE	0.14	0.14	0.15	0.06
	0.37	0.36	0.33	1.00
REnV.NTT / REnV.T0	0.10	0.14	0.14	0.19
	0.64	0.26	0.27	0.07

Table 24. As in Table 18, except for REnV arrays.

	n = 5	n = 7	n = 9	n = 11
REnV.NTM / REnV.MALL	No	No	No	No
REnV.NTM / REnV.MPRE	No	No	No	No
REnV.NTM / REnV.M0	No	No	No	No
REnV.NTT / REnV.TALL	No	Yes 2 < 1.06	Yes 2 <1.02	Yes 2 <0.62
REnV.NTT / REnV.TPRE	Yes 2 < 0.78	Yes 2 < 0.81	Yes 3 < 0.30	No
REnV.NTT / REnV.T0	No	No	No	No

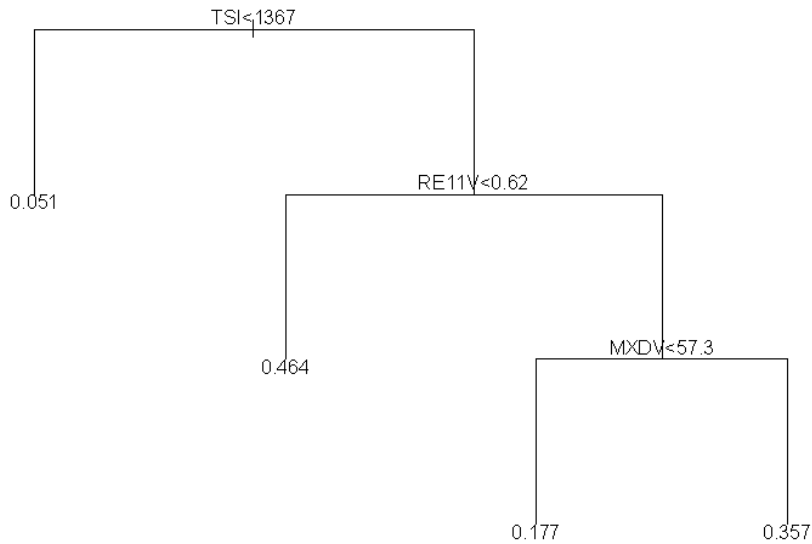


Fig. 44. NTT versus TALL regression tree using SSAP TVS parameters from Table 6 with RE11V.

To determine whether REV arrays provide better predictive skill than SW, additional regression trees were constructed using combinations of the SSAP, RE and SW parameters. Both Reflectivity and SW had to appear in the original comparisons (Table 18 and Table 24) for

that array size to be considered. Table 25 summarizes results for these comparisons. REV is selected over SW in every case, except for the NTT versus T0 comparison at array size 9 where both REV and SW are selected (Fig. 45). Therefore, I conclude that REV shows predictive skill in regression trees that is superior to both SW and AZ.

These results indicate that REV shows promise as an additional source of information for diagnosing tornadoes, especially when used with the Tornado Detection Algorithm. When REV is used by itself, it fails to show skill at discriminating between tornadic and non-tornadic detections. However, when combined with other predictors in TVS regression trees, small values of REV became significant predictors of tornadic TVSSs. Several studies (e.g., Howell and Beaman 2006) have documented a reduction in horizontal reflectivity gradient during the onset of a tornado, so decreasing REV could be a useful predictor of a developing tornado, or an indicator of one that already is occurring.

Table 25. Results for regression trees including SWn and REnV arrays. The first line indicates whether REV or SW appears in the regression tree. The second line indicates at which split the parameter occurs. The third line indicates the threshold of the split.

	n = 7	n = 9	n = 11
NTT - TALL		REV 3 <1.02	REV 2 < 0.62
NTT - T0	RE7V 2 <0.19	REV / SW 2 / 2 < 0.99 / < 4.1	REV 2 < 1.74

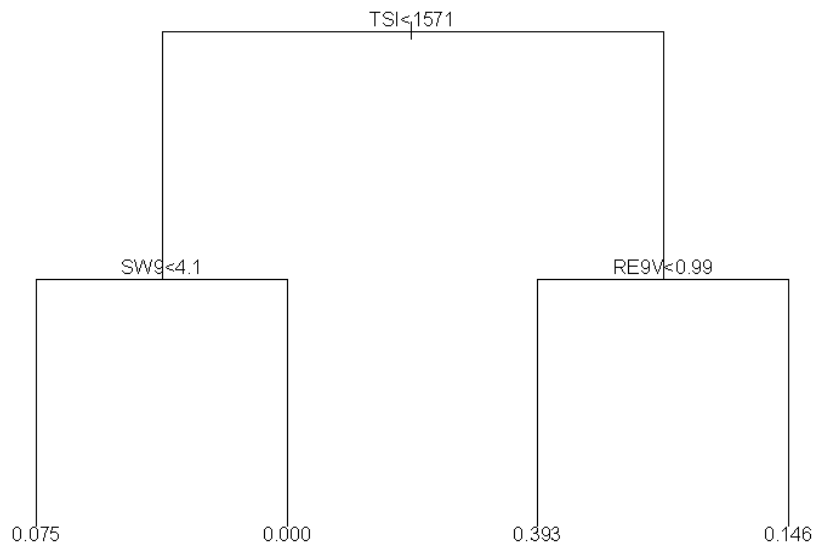


Fig. 45. NTT versus T0 regression tree using SSAP TVS parameters from Table 6 with SW9 and RE9V.

CHAPTER 4 SUMMARY AND CONCLUSIONS

The Weather Surveillance Radar – 1988 Doppler (WSR-88D) is the primary means by which tornadoes are detected by the National Weather Service. The existence of tornadoes can be inferred by algorithms that identify mesocyclones or Tornado Vortex Signatures (TVSs) within the velocity data. Unfortunately, most mesocyclones are not associated with tornadoes, and there is a large false alarm rate with the TVSs. Several previous studies have shown that the diagnostic parameters within the Mesocyclone or TVS Detection Algorithms (MDA and TDA, respectively) exhibit comparable skill to the algorithms themselves as tornado predictors (e.g., Watson et al. 2005; Marzban 2001; Turnage et al. 2000; Jones et al. 2004).

The WSR-88D provides information other than just the velocity data used by the mesocyclone and TVS detection algorithms. Specifically, Reflectivity and Spectrum Width are computed along with Velocity; however, there is no operationally available way to associate these parameters with the algorithms. I used the Warning Decision Support System – Integrated Information (WDSSII) software package to make associations with archived data.

Several studies (e.g., Trapp et al. 1999; Funk et al. 1999) have shown that many radar-observed tornadic circulations originate in the lowest levels of thunderstorms. These circulations then rapidly strengthen and stretch upward with the onset of the tornado. This differs from the classical radar-observed tornadogenesis paradigm in which the strongest circulations originate in the middle levels of a storm as a mesocyclone and then stretch and intensify toward the surface as a tornado. Numerical simulations have shown the strongest rotation with the non-descending mode of tornadogenesis begins and remains in the lowest levels of the storm.

Tornadoes in the southeastern United States frequently occur with quasi-linear convective systems (QLCSs). Tessendorf and Trapp (2000) have shown the non-descending mode of tornadogenesis is especially common with QLCSs. Due to the frequent low-level origin and rapid onset of QLCS tornadoes, it is difficult to issue timely tornado warnings for them, even though numerical simulations suggest that the strength and general dimensions of the QLCS mesocyclone approximate those of the classical tornado mesocyclone.

The first part of this study identified 86 tornadoes that occurred during 22 separate severe weather episodes primarily in the southeastern United States. Archived radar data from the nearest WSR-88D were collected for each event. Storm Data reports and subjective analyses of radar data then were used to determine the exact times of tornado occurrences. Unfortunately, storm reports can be erroneous in time and/or space. Once the radar datasets were adjusted to

be centered near the corrected times of tornado occurrence, the MDA and TDA algorithms were executed to detect mesocyclones and TVSSs within the Velocity data. Most of the algorithms' detections were not associated with a reported quasi-linear convective system tornado. Therefore, the Storm Data tornado location reports were compared to the mesocyclone and TVSS detection locations to discriminate between the tornadic and pre-tornadic mesocyclone or TVSS detections from the non-tornadic (null) detections.

Once datasets of tornadic and non-tornadic detections were compiled, selected diagnostics from the MDA and TDA were compared with the tornadic and non-tornadic datasets. Diagnostics of Low Level Delta Velocity (LLDV), Low-Level Rotational Velocity (LLROTV), and Strength Index showed some skill at discriminating between the tornadic and non-tornadic mesocyclones. However, the remainder of the selected mesocyclone parameters showed no significant skill, and none of the TVSS parameters showed significant skill at discriminating between the tornadic, non-tornadic, or pre-tornadic cases. In the case of mesocyclones, the correlation coefficient was 0.803 between LLDV and Maximum Delta Velocity for the pre-tornadic detections. This suggested that most of the tornadoes followed the non-descending tornadogenesis paradigm. The correlation coefficient between the pre-tornadic LLROTV and Maximum Rotational Velocity detections was ~ 0.74 ; however, this smaller value can be explained by sampling errors that can be more significant with the Rotational Velocity diagnostic.

Since none of the individual diagnostics showed significant skill at discriminating between the tornadic and non-tornadic detections, combinations of parameters were selected using the regression tree approach to determine whether better skill could be achieved. Because undesirable co-linearity effects can occur between highly correlated parameters, the list of MDA and TDA parameters was trimmed to eliminate those parameters showing the greatest correlations with each other. Ten-fold cross validation tests were performed on the remaining parameters to determine the maximum number of terminal nodes at which the regression trees would still generalize to independent data. Predictors such as Vertically Integrated Rotational Velocity and LLDV often were selected for the trees, suggesting that they were sufficiently pruned to generalize to different datasets. These combinations of predictors sometimes produced detection success rates greater than 30%, thereby exceeding the success rates of individual MDA or TDA parameters. In these cases, the combination of predictors did yield greater success rates.

Next, the operationally unavailable parameters Spectrum Width (SW), Reflectivity Variance (REV), and Azimuthal Shear (AZ) were analyzed to determine if they contributed additional predictive skill compared to the diagnostic parameters alone. This part of the study was unique since no prior studies have attempted to determine whether selected properties of SW, RE, or AZ could discriminate between quasi-linear tornadic mesocyclones and TVSSs of the non-

tornadic variety.

Comparative box plots of SW showed that largest values generally occurred with the non-tornadic detections, closely followed by the tornadic detections. This unexpected result suggests that the pre-tornadic circulations might exhibit relatively small turbulent helical flow prior to stretching and shrinking into a tornadic state, at which time the turbulence increases to make the differences negligible between the NTM and NTT detections. Various size arrays for computing SW were considered. Qualitatively, the differences in SW between the tornadic and non-tornadic datasets were too small to be useful operationally. Two-sample Kolmogorov-Smirnov goodness of fit tests also showed little if any statistically significant differences among the tornadic, pre-tornadic, and non-tornadic datasets. Generally, qualitative differences were smallest with the largest arrays. SW arrays next were included in the regression trees to determine whether they would yield predictive skill comparable to the best performing MDA and TDA diagnostics. For the mesocyclone detections, the predictors VIROTV and LLDV always dominated over every SW array size. For the TVS comparisons, only the larger SW arrays appeared in some trees. This suggests that the larger SW arrays had predictive ability that was comparable to the four TDA predictors used in the regression trees

Azimuthal Shear (AZ) frequently was found to exhibit negative values, even during tornado occurrences. This result was unexpected since mesocyclones and TVSs are almost always associated with positive shear. Different array sizes of AZ showed strong correlations with each other, which was expected since the linear least squares derivative that is applied to the Velocity data has an *a priori* smoothing effect. Two-tailed two-sample Kolmogorov-Smirnov goodness of fit tests showed that the most statistically significant differences occurred between the non-tornadic (NTM) and tornadic (M0) AZ datasets, as well as between the NTM and tornadic/pre-tornadic (MALL) datasets. There were a few cases where statistically significant differences existed between the non-tornadic TVS (NTT) versus tornadic/pre-tornadic TVS (TALL) datasets. Every other comparison did not meet the 0.05 confidence threshold. These results indicate that AZ exhibited slightly better statistical ability than SW at discriminating between tornadic and non-tornadic mesocyclones. When used in regression trees together with MDA and TDA parameters, AZ exhibited utility comparable to SW for TVS detections and was superior to SW for mesocyclone detections. When both SW and AZ arrays were used to create regression trees, SW always emerged as the dominant predictor. A surprising finding was the preponderance of negative AZ values in the tornadic TVS detections. Conversely, the non-tornadic TVS detections were predominantly positive. There currently is no good explanation for why the tornadic TVS detections have a strong negative mode.

Reflectivity Variance (REV) was the final new parameter to be investigated. Pronounced differences were observed among the different array sizes, and these were confirmed by smaller

correlation coefficients among the arrays. This indicates a greater likelihood of extracting different results with increasing array size. Since there is an upper limit of variance with increasing array size, REV array sizes appeared to have an upper limit of usefulness. Contrary to what was hypothesized, pre-tornadic mesocyclone and TVS detections showed larger variance than tornadic detections. One possible reason is that mesocyclone occlusion during tornadogenesis may reduce the reflectivity gradient that has been observed prior to the tornado. However, this would not explain why the same trend was not observed with the TVS detections. Two-sample Kolmogorov-Smirnov goodness of fit tests revealed that the most statistically significant differences existed between the NTM and MPRE datasets. When used in regression trees, REV did not exhibit skill comparable to the best SSAP diagnostics for the mesocyclone detections. However for TVS detections, larger arrays of REV appeared in regression trees for the NTT versus TALL comparisons, and smaller arrays appeared in regression trees for the NTT versus TPPE comparisons. Regression trees were constructed using the REV arrays together with the best-performing MDA and TDA predictors. Whenever REV appeared in a decision tree, it nearly always was located at the second split instead of the third split, as was observed with SW. This suggested that REV had better predictive ability for the TVS datasets than did SW. To test this inference, new regression trees were constructed using similar sizes of SW and REV arrays to determine which parameter would be selected. Results revealed that REV was selected over SW in every case, except for one in which both REV and SW were selected. This strongly suggests that REV exhibited predictive skill in the regression trees that was superior to both SW and AZ.

The regression trees into which the new parameters were incorporated suggest that SW, AZ, and REV all show utility as predictors when used in combination with some of the already existing MDA and TDA diagnostic parameters. The results of this study indicate that the ability of current operational mesocyclone and TVS detection algorithms to discriminate between tornadic and non-tornadic detections could be improved by implementing SW, AZ, or REV data into the algorithms. This improvement would provide operational forecasters with better tools for making critical tornado warning decisions.

REFERENCES

- Brieman, L., Friedman, J. H., Olshen, R. A., and C. A. Stone, 1984: *Classification and Regression Trees*. CRC Press, 358 pp.
- Brown, R. A., L. R. Lemon, and D. W. Burgess, 1978: Tornado detection by pulsed Doppler radar. *Mon. Wea. Rev.*, **106**, 29-39.
- Crawley, M. J., 2002: *Statistical Computing: An Introduction to Data Analysis using S-Plus*. John Wiley & Sons Ltd. Press, 761 pp.
- Crum, T. D., and R. L. Alberty, 1993: The WSR-88D and the WSR-88D Operational Support Facility. *Bull. Amer. Meteor. Soc.*, **74**, 1669-1687.
- Crum, T. D., and D. W. Burgess, 1993: Recording, archiving, and using WSR-88D data. *Bull. Amer. Meteor. Soc.*, **74**, 645--653.
- Distance Learning Operations Course (DLOC), NOAA/NWS Warning Decision and Training Branch. Available online at:
<http://www.wdtb.noaa.gov/Courses/dloc/topic5/Topic5.pdf>
- Funk, T. W., K. E. Darmofal, J. D. Kirkpatrick, V. L. DeWald, R. W. Przybylinski, G. K. Schmoker, and Y. J. Lin, 1999: Storm reflectivity an mesocyclone evolution associated with the 15 April 1994 squall line over Kentucky and southern Indiana. *Wea. Forecasting*, **14**, 976 - 993.
- Herald, P. and K. Drozd, 2001: Use of spectrum width and combined shear in tornado detection. NOAA NWS Central Region Applied Research Paper 24-06.
- Howieson, E. D., B. Grant, G. J. Stumpf, and D. W. Effertz, 1997: Doppler radar algorithm performance during a highly sheared tornado outbreak. Preprints, *28st Conf. on Radar Meteor.* Austin, TX, Amer. Meteor. Soc., 540-541.
- Jones, T. A., K. M. Mcgrath, and J. T. Snow, 2004: Association between NSSL Mesocyclone Detection Algorithm – detected vortices and tornadoes. *Wea. Forecasting*, **19**, 872 - 890.
- Howell, J. L. and J. F. Beaman, 2006: Mini-supercell event of 23 October 2004 in the Memphis county warning area. *Natl. Wea. Assoc. Electronic Jour. of Oper. Met.*, **7**, 40 pp.
<http://www.nwas.org/ej/2006-EJ6/>
- Lakshmanan, V., 2002: WDSSII: an extensible, multi-source meteorological algorithm development interface. Preprints, *21st Conf. on Severe Local Storms*, San Antonio, TX, Amer. Meteor. Soc., 134-137.
- Lee, R.R., G.J. Stumpf, and P.L. Spencer, 1998: Should Geographic Region or Near-storm Environment Dictate WSR-88D Algorithm Adaptable Parameter Settings? Preprints, *19th Conf. on Severe Local Storms*, Minneapolis, MN, Amer. Meteor. Soc., 784-787.
- Lemon, L. R., 1980: Severe thunderstorm radar identification techniques and warning criteria. NOAA Tech. Memo. NWS NSSFC-3, NSSL, Kansas City, 60 pp. [U.S. Department of Commerce, Sills Building, 5285 Port Royal Road, Springfield, VA 22151].
- Leslie, L. M., 1971: The development of concentrated vortices: A numerical study. *J. Fluid Mech.*, **48**, 1-21.
- Manross, K. L., Robert J. Trapp, and Gregory J. Stumpf, 2003: WSR-88D radar characteristics of

- quasi-linear convective system tornadoes using the NSSL Severe Storm Analysis Program. Preprints, *31st Conf. On Radar Meteorology*, Seattle Washington, Amer. Meteor. Soc.
- Marzban, C., Mitchell, E. D., and G. J. Stumpf, 1999: The notion of "best predictors": an application to tornado prediction. *Wea. Forecasting*, **14**, 1007 - 1016.
- Marzban, C., 2001: Tornado warning guidance based on an analysis of MDA/TDA/NSE data. [Available online at <http://www.wdtb.noaa.gov/modules/twg02/twg2001stats.pdf>]
- McAvoy, B. P., W. A. Jones, and P. D. Moore, 2000: Investigation of an unusual storm structure associated with weak to occasionally strong tornadoes over the eastern United States. Preprints, 20th Conf. on Sev. Local Storms, Orlando, FL, Amer. Meteor. Soc.
- Mitchell, E. D., S. V. Vasiloff, G. J. Stumpf, A. Witt, M. D. Eilts, J. T. Johnson, and K. W. Thomas, 1998: The National Severe Storms Laboratory Tornado Detection Algorithm. *Wea. Forecasting*, **13**, 352 - 366.
- Morgan, C., J. Orrock, N. Rydell, and J. Ward, 1998: A meteorological and radar analysis of the central Texas tornado outbreak on May 27, 1997 NOAA Tech. Memo. NWS SR-198.
- Smith, T. M., K. L. Elmore, G. J. Stumpf, and V. Lakshmanan, 2003: Detection of rotation and boundaries using two-dimensional, local, linear least squares of velocity derivatives. Preprints, 31st Conf. on Radar Meteorology, Seattle, WA, Amer. Met. Soc., 310-313.
- Stumpf, G. J., A. Witt, E. D. Mitchell, P. L. Spencer, J. T. Johnson, M. D. Eilts, K. W. Thomas, and D. W. Burgess, 1998: The National Severe Storms Laboratory Mesocyclone Detection Algorithm. *Wea. Forecasting*, **13**, 304 - 326.
- Tessendorf, S. A., and R. J. Trapp, 2000: On the climatological distribution of tornadoes within quasi-linear convective systems. Preprints, 20th Conf. on Sev. Local Storms, Orlando, FL, Amer. Meteor. Soc., 134-173.
- Trapp, R. J., and R. Davis-Jones, 1997: Tornadogenesis with and without a dynamic pipe effect. *J. Atmos. Sci.*, **54**, 113-133.
- Trapp, R. J., E.D. Mitchell, G.A. Tipton, D. W. Effertz, A. I. Watson, D. L. Andra Jr., and M. A. Magsig, 1999: Descending and Nondescending Tornadoic Vortex Signatures Detected by WSR-88Ds. *Wea. Forecasting*, **14**, 625 -639.
- Trapp, R. J., and M. L. Weisman, 2000: Preliminary Investigation of Tornadogenesis within Quasi-Linear Convective Systems. Preprints, 20th Conf. on Sev. Local Storms, Orlando Florida, Amer. Meteor. Soc., 273 - 276.
- Trapp, R. J., G. J. Stumpf, and K. L. Manross, 2005: A reassessment of the percentage of tornadic mesocyclones. *Wea. Forecasting.*, **20**, 680-687.
- Turnage, T. J., R. R. Lee, and E. D. Mitchell, 2000: WSR-88D Mesocyclone Characteristics of Selected Thunderstorms during the Southwest Georgia Tornado Outbreak of 13-14 February 2000: An Overview. Preprints, 20th Conf. on Sev. Local Storms, Orlando Florida, Amer. Meteor. Soc., 364 - 367.
- Turnage, T.J., 2001: Utilizing the Warning Decision Support System for detecting tornadoes associated with Tropical Storm Helene. Preprints, 18th Conf. on Weather Analysis and Forecasting, Ft. Lauderdale, FL, Amer. Met. Soc.
- Venables, W. N., and B. D. Ripley, 1997: *Modern Applied Statistics with S-PLUS*. Springer-Verlag, New York, 548 pp.

- Wakimoto, R. M., C. Liu, and H. Cai, 1998: The Garden City , Kansas, storm during VORTEX 95. Part I: Overview of the storm's life cycle and mesocyclogenesis. *Mon. Wea. Rev.*, **126**, 372-392.
- Watson, A. I., M. A. Jamski, T. J. Turnage, J. R. Bowen, and J. C. Kelley, 2005: The tornado outbreak across the north Florida panhandle in association with hurricane Ivan. Preprints, 32nd Conf. on Radar Meteorology. Albuquerque, NM, Amer. Met. Soc.
- Weisman, M. L. and J. B. Klemp, 1982: The dependence of numerically simulated convective storms on vertical wind shear and buoyancy. *Mon. Wea. Rev.*, **110**, 504-520.
- Weisman, M. L. and R. J. Trapp, 2003: Low-level mesovortices within squall lines and bow echoes. Part I: Overview and dependence on environmental shear. *Mon. Wea. Rev.*, **131**, 2779-2803.
- Welsh, P., 1997: Lessons learned in configuring and using the NEXRAD (WSR-88D) radar for detection of tropical cyclone induced tornadoes (tcit). Preprints, 28st Conf. on Radar Meteor. Austin, TX, Amer. Meteor. Soc., 582-583.
- Witt, A., M. D. Eilts, G. J. Stumpf, E. D. Mitchell, J. T. Johnson, and K. W. Thomas, 1998: Evaluating the performance of WSR-88D severe storm detection algorithms. *Wea. Forecasting*, **13**, 513 - 518.
- Zittel, W. D., Lee, R. R., Mitchell, E. D., and D. Sirmans, 2001: Environmental and signal processing conditions that negatively impact the performance of the WSR-88D tornado detection algorithm. Preprints, 30th International Conf. on Radar Meteor. Munich, Germany, Amer. Meteor. Soc.

BIOGRAPHICAL SKETCH

Thomas James (T. J.) Turnage was born in Silver Spring, Maryland on October 3rd, 1967. After moving to Ames, Iowa in 1971, he had the opportunity to witness the many types of extreme weather that the Midwest had to offer, which resulted in a lifelong interest in meteorology. A particularly influential event was the F5 Jordan, Iowa tornado that occurred on June 13, 1976 less than 10 miles from his home.

After graduating from Ames High School in 1986, T. J. attended Iowa State University and graduated with a B. S. in Meteorology in Spring of 1991. Shortly after graduation, T. J. began his career with the National Weather Service (NWS) as an intern in Midland, Texas, where he was later promoted to a forecaster position. In November of 1998, T. J. took a promotion to senior forecaster in Tallahassee, Florida. Shortly after his move, he met his future wife, Sarah. In Spring of 2000, T. J. began graduate work while continuing his duties as a full-time operational forecaster. His family grew to include two children and several cats and dogs.

In November of 2005, T.J. was selected to be the new Science and Operations Officer at the NWS office in Grand Rapids, Michigan. This fulfilled a career-long dream of occupying this position and returning north to experience four distinct seasons in the Midwest once again.